Ph.D. Dissertation of Engineering

Modeling of CFRTP Composites Manufacturing Process with In-Situ Polymerization

현장중합을 이용한 CFRTP 복합재료 성형 공정의 모델링에 대한 연구

February 2017

Graduate School of Engineering

Seoul National University

Department of Mechanical & Aerospace Engineering

Li Meixian

Modeling of CFRTP Composites Manufacturing Process with In-Situ Polymerization

Academic advisor Prof. Woo Il Lee

Submitting a Ph.D. Dissertation of Engineering

November 2016

Graduate School of Engineering
Seoul National University
Department of Mechanical & Aerospace Engineering

Li Meixian

Confirming the Ph.D. Dissertation written by
Li Meixian
December 2016

Chair	Maeng Hyo Cho (Seal)
Vice Chair	Woo Il Lee (Seal)
Examiner	Charn Jung Kim (Seal)
Examiner	Sung Hoon Ahn (Seal)
Examiner	Sun Kyoung Kim (Seal)

Abstract

Modeling of CFRTP Composites Manufacturing Process with In-Situ Polymerization

Li Meixian

Department of Mechanical and Aerospace Engineering

The Graduate School

Seoul National University

Recently, research on thermoplastic composites has greatly increased due to their desirable properties such as high specific strength, impact resistance, recyclability and so on. However, because of its high melt viscosity, manufacturing processes of thermoplastic composites have been limited, such as extrusion, injection molding, and compression molding. These manufacturing techniques need high fabricating temperature and pressure, and moreover some of the techniques are just compatible for short length fibers with low volume fraction; therefore, it has also limited wider applications of thermoplastic composites. Since the requirements of thermoplastic composites increase, low-

cost manufacturing technique with high fiber volume fraction needs to be developed.

In this study, vacuum assisted resin transfer molding (VaRTM), which is one of the liquid molding process, was used for fabrication of thermoplastic composites. Generally, VaRTM is a low-cost manufacturing technique for thermoset resin composites; however, it is not compatible for thermoplastic resin with high melt viscosity. Therefore, low viscosity monomer, which is a molecule that may bind chemically to other molecules to form a polymer, was used as resin to fabricate thermoplastic composites via VaRTM method.

Polyamide 6 (PA6) is one of the main engineering plastics used for a wide range of applications, and its monomer called ε-caprolactam has low viscosity even at low temperatures; therefore, it is easily molded than other thermoplastics. During VaRTM process, ε-caprolactam can be polymerized to PA6 with catalyst, activator and a specific molding temperature. Degree of polymerization usually depends on sorts of catalysts and activators, molding temperatures and the ratio of monomer/catalyst/activator. In this study, only one type of catalyst and activator was used, and their weight ratio was fixed. In other words, molding temperature was the only parameter for polymerization of ε-caprolactam. According to the experimental findings, at 140℃ molding temperature, the monomer was polymerized very well and the resin impregnation was also very good. Furthermore, bending strength, bending modulus and impact strength of

the specimens at 140℃ show the best values among those of other samples molded at other temperatures.

Another purpose of this study is to evaluate the polymerization kinetics of ε-caprolactam. However, polymerization and crystallization of ε-caprolactam occurs nearly simultaneously, so it is difficult to investigate polymerization and crystallization kinetics. Thus, the polymerization and crystallization process with different heating rates were separated using Gaussian and Maxwell-Boltzmann distribution in order to study only the polymerization kinetics. Modeling results showed that the first order autocatalytic reaction model presents a very good fitting, namely, the model is suitable for describing the polymerization kinetics of ε-caprolactam. Furthermore, process parameters are also proposed by comparison of simulation results and experimental results.

Keywords: ε-Caprolactam, Vacuum assisted resin transfer molding (VaRTM), Differential scanning calorimeter (DSC), Polymerization kinetics, Crystallinity

Student Number : 2011-31286

CONTENTS

ABSTRACT ..... **II**

LIST OF FIGURES ..... **VIII**

LIST OF TABLES ..... **XIII**

CHAPTER 1. INTRODUCTION **1**

1.1 OVERVIEW AND PROBLEM DESCRIPTION 1

1.2 LITERATURE REVIEW 8

1.3 OBJECTIVE OF RESEARCH 11

1.4 OUTLINE OF DISSERTATION 13

CHAPTER 2. MATERIALS AND PROCESS **14**

2.1 MATERIALS 17

2.1.1 Monomer ***17***

2.1.2 Catalyst and activator *18*

2.1.3 Reinforcement *19*

2.2 SETTING AND PROCESS 21

2.2.1 Experimental setting *21*

2.2.2 Experimental process *23*

2.3 CHARACTERIZATION METHODS 24

2.3.1 Mechanical properties *24*

2.3.2 Differential scanning calorimetry (DSC) analysis *26*

CHAPTER 3. MECHANICAL PROPERTIES **30**

3.1 MEASUREMENT OF UNREACTED MONOMER AND WATER ABSORPTION ... 30

3.2 THREE POINT BENDING TEST 33

3.3 IZOD IMPACT TEST 35

3.4 SCANNING ELECTRON MICROSCOPE (SEM) OBSERVATION 37

3.5 CRYSTALLINITY OF CFRTP COMPOSITES 40

CHAPTER 4. INVESTIGATION OF POLYMERIZATION KINETICS .. **44**

4.1 DYNAMIC SCANNING 45

4.1.1 Analysis of polymerization kinetics at different heating rates *45*

4.1.2 Separation of polymerization and crystallization curves *48*

4.1.3 Modeling of polymerization kinetics at different heating rates *52*

4.2 ISOTHERMAL SCANNING 60

4.2.1 Scanning process *60*

4.2.2 Analysis of polymerization kinetics during isothermal scanning....60

CHAPTER 5. NUMERICAL ANALYSIS 66

5.1 Governing equations and methods 66

5.2 Simulation results.....77

5.2.1 Flow in a rectangular mold 77

5.2.2 Flow in an automotive part with one or three inlets.....81

SUMMARY AND CONCLUSIONS.....91

BIBLIOGRAPHY 94

초 록 102

List of Figures

Figure 1. 1 Replacement parts of automotive using CFRP (Reproduced from [1])

Figure 1. 2 CFRTS composites via HPRTM technology <BMW i8 sideframe> [3]

Figure 1. 3 Melt viscosities and processing temperature of various matrix materials for both reactive and melt processing (Reproduces from [6])

Figure 1. 4 Development tendency of performance, price, and cycle time of CFRP composites for automotive parts

Figure 1. 5 Factors that affect polymerization kinetics

Figure 1. 6 Schematic illustration of T-RTM

Figure 1. 7 Research objective

Figure 2. 1 Schematic illustration of the manufacturing process for thermoplastic resin

Figure 2. 2 Formula of ε-caprolactam

Figure 2. 3 Anionic polymerization of ε-caprolactam

Figure 2. 4 Carbon fabric used in this study

Figure 2. 5 Schematic illustration of the VaRTM process

Figure 2. 6 Design for lower mold

Figure 2. 7 Photographs of fabricated CFRTP composites

Figure 2. 8 Device for three point bending test and izod impact test

Figure 2. 9 Schematic illustration of differential scanning calorimetry

Figure 2. 10 Differential scanning calorimetry (DSC) device

Figure 3. 1 Content of unreacted monomer of pure PA6 and CFRTP composites

Figure 3. 2 Content of water absorption of pure PA6 and CFRTP composites

Figure 3. 3 Bending strength and modulus of pure PA6 and CFRTP at different molding temperatures

Figure 3. 4 Impact strength of pure PA6 at different molding temperatures

Figure 3. 5 Impact strength of CFRTP at different molding temperatures

Figure 3. 6 SEM micrograph of the fracture surface of CFRTP at different molding temperatures. (a) 120℃, (b) 140℃, (c) 160℃, (d) 180℃, and (e) 200℃

Figure 3. 7 DSC thermograms of the molded samples

Figure 3. 8 Degree of crystallinity for pure PA6 and CFRTP composites at different molding temperatures

Figure 4. 1 DSC thermograms of caprolactam at five different heating rates

Figure 4. 2 Crystallinity at different heating rates during polymerization

Figure 4. 3 Polymerization at different heating rates

Figure 4. 4 Separation of polymerization and crystallization curve at different heating rates. (a) 10℃/min, (b)15℃/min, (c)20℃/min, (d)30℃/min, (e)50℃/min [40]

Figure 4. 5 Comparison of modeling results with experimental data using the 1st order autocatalytic reaction model

Figure 4. 6 Kinetic parameters for polymerization of ε-caprolactam at different heating rate.

Figure 4. 7 Comparison of modeling results with experimental data using exponential fitting parameters

Figure 4. 8 DSC thermograms of isothermal scanning process

Figure 4. 9 DSC diagrams of the first heating process

Figure 4. 10 DSC diagrams of the second heating process

Figure 5. 1 Schematics of volume of fluid (VOF) method

Figure 5. 2 Illustration for porous media flow

Figure 5. 3 Viscosity-time profile of CL/C1/C20 (100/4/4) at 150℃ [49]

Figure 5. 4 Viscosity-time profile of ε-caprolactam during the first 30 seconds at different temperatures

Figure 5. 5 Viscosity-time profile of ε-caprolactam during the first 20 seconds at different temperatures

Figure 5. 6 Relationship between filling time and parameter of viscosity

Figure 5. 7 Critical time at different molding temperatures

Figure 5. 8 Geometry of rectangular mold

Figure 5. 9 Simplified mold

Figure 5. 10 Phase contours in carbon fabric with various molding temperatures

Figure 5. 11 Relationship between filling time and filling ratio at different molding temperatures

Figure 5. 12 Geometry of automotive part with one inlet

Figure 5. 13 Geometry of automotive part with three inlets

Figure 5. 14 Phase contours in CFRTP composites with one inlet at 10 bar

Figure 5. 15 Phase contours in CFRTP composites with one inlet at 20 bar

Figure 5. 16 Phase contours in CFRTP composites with one inlet at 30 bar

Figure 5. 17 Phase contours in CFRTP composites with one inlet at 40 bar

Figure 5. 18 Phase contours in CFRTP composites with one inlet at 50 bar

Figure 5. 19 Phase contours in CFRTP composites with one inlet at 60 bar

Figure 5. 20 Phase contours in CFRTP composites with three inlets at 10 bar

Figure 5. 21 Phase contours in CFRTP composites with three inlets at 20 bar

Figure 5. 22 Phase contours in CFRTP composites with three inlets at 30 bar

Figure 5. 23 Phase contours in CFRTP composites with three inlets at 40 bar

Figure 5. 24 Phase contours in CFRTP composites with three inlets at 50 bar

List of Tables

Table 2. 1 Viscosity of polymers at a specified temperature

Table 2. 2 Specification of carbon fabric

Table 3. 1 Degree of crystallinity for pure PA6 and CFRTP composites at different molding temperatures

Table 4. 1 The values of heat of fusion during heating process

Table 4. 2 Reaction parameters of the polymerization kinetics at different heating rates

Table 4. 3 Reaction parameters of the polymerization kinetics at different heating rate using exponential curves in Figure 4. 6

Table 4. 4 DSC diagrams of isothermal scanning process

Table 4. 5 DSC diagrams of the first heating process

Table 4. 6 DSC diagrams of the second heating process

Table 5. 1 Filling time and filling ratio at different pressures with one inlet

Table 5. 2 Filling time and filling ratio at different pressures with three inlets

CHAPTER 1. Introduction

1.1 Overview and problem description

Recently, development of lightweight vehicle has increasingly drawn in the face of strict regulations on fuel economy and carbon dioxide emissions. For the weight reduction of vehicle, carbon fiber reinforced plastics (CFRP) is a promising material due to its high specific strength. Nowadays CFRP composites have been used for the production of panels, modules, structures, and other parts (Figure 1. 1). As shown in Figure 1. 1, some parts (door frame, seat, energy absorption pipe, FR dash, under cover, door inner & impact beam) are made of continuous fiber, while the other parts are made of discontinuous CFRP. As Toray proposed, body weight can be reduced from 1380kg to 970kg after using CFRP composites instead of metal materials, which can lead to better fuel economy [1].

Generally, CFRP can be divided into carbon fiber reinforced thermoset (CFRTS) composites and carbon fiber reinforced thermoplastic (CFRTP) composites, depending on the type of polymers used as matrixes.

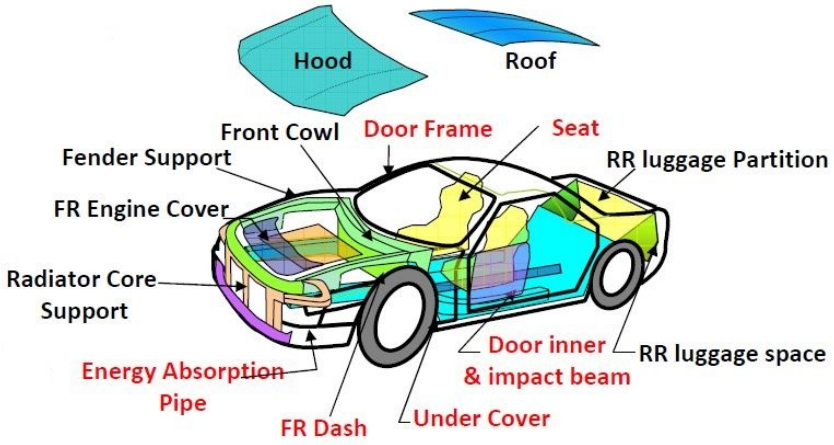

Figure 1. 1 Replacement parts of automotive using CFRP (Reproduced from [1])

Takahashi et al. [2] reported that the weight of CFRTS or CFRTP composites is 1/3 of steel panel, whereas elastic strain of CFRTS and CFRTP is about 4 times of that of steel panel. Moreover, flexural modulus of both unidirectional CFRTS and CFRTP is similar to that of steel panel, while flexural strength of both unidirectional CFRTS and CFRTP is about 3 times higher than that of steel panel. In addition, specific flexural stiffness and specific flexural strength of CFRP composites are much higher than those of steel panel due to low density of CFRP composites. Therefore, it can be inferred that CFRP composites have good mechanical properties to replace some metal parts of automobile.

Traditionally, CFRTS composites have been widely used for structural applications due to their good mechanical properties and thermal stability. In

recent years, high pressure resin transfer molding (HPRTM) technology has been used for CFRTS composites to reduce cycle time (Figure 1. 2), and it is already being used in series production of structural carbon fiber reinforced plastic parts in BMW's (Munich, Germany) i3 and i8 models [3]. The difference between HPRTM and RTM is that the cycle time of HPRTM is much faster than standard RTM. Depending on part size and geometry, cycle time of standard RTM is 30 to 60 minutes with 10 to 20 bars injection pressure, whereas that of HPRTM is less than 10 minutes with 20 to 120 bars injection pressure and up to 150 bars pressure in the mixing head. For automotive industry, reduction of cost and cycle time is a key issue, thus research on fast cure resin like fast cure epoxy has been carried out these days. According to the reports from BMW, they have already produced the parts for i3 and i8 with less than 10 minutes cure cycle. Consequentially, only 1000 to 4000 parts were produced per year, while 12000 to 50000 parts are produced per year now [4, 5]. However, high pressure over 100-110 bar may cause washout of carbon fiber preform and prepreg, moreover, low processability and recyclability of thermoset polymers limit their mass productions.

Recently, CFRTP composites are considered to be a better alternative for applications of CFRPS in mass productions because of its potential for high processability and recyclability. In terms of processability, cycle time of CFRTP is faster over that of CFRTS. Considering recyclability, thermosetting polymers once cured, can neither be reheated nor reshaped, and heating cured thermosetting polymers will only result in char, whereas thermoplastic polymers

can be reheated and reshaped number of times which makes carbon fiber reinforced thermoplastics (CFRTP) highly recyclable.

Figure 1. 2 CFRTS composites via HPRTM technology <BMW i8 sideframe> [3]

However, compared to thermoset polymers, high viscosity of thermoplastic polymers requires high temperature and high pressure for the materials to be impregnated to carbon fiber reinforcements. For example, thermosetting polymers, such as epoxy, can be impregnated to carbon fiber reinforcements and cured below 200℃. However, thermoplastic polymers must be heated to melting temperature, which is typically well above 200℃, and require high pressures (10 to 50 bars) to be impregnated to carbon fiber reinforcements.

In order to prevent fiber misalignment and to improve preform permeability, thermoplastic RTM (T-RTM) which is called in situ polymerization technique is developed. Monomers with catalysts and activators start to be polymerized during injection process. On the one hand, fast polymerization is one of the advantages for reduction of cycle time, but on the other hand, it is difficult to deal with the molding process due to fast gel time of polymerization. Therefore, it is a challenge to control polymerization time of monomers.

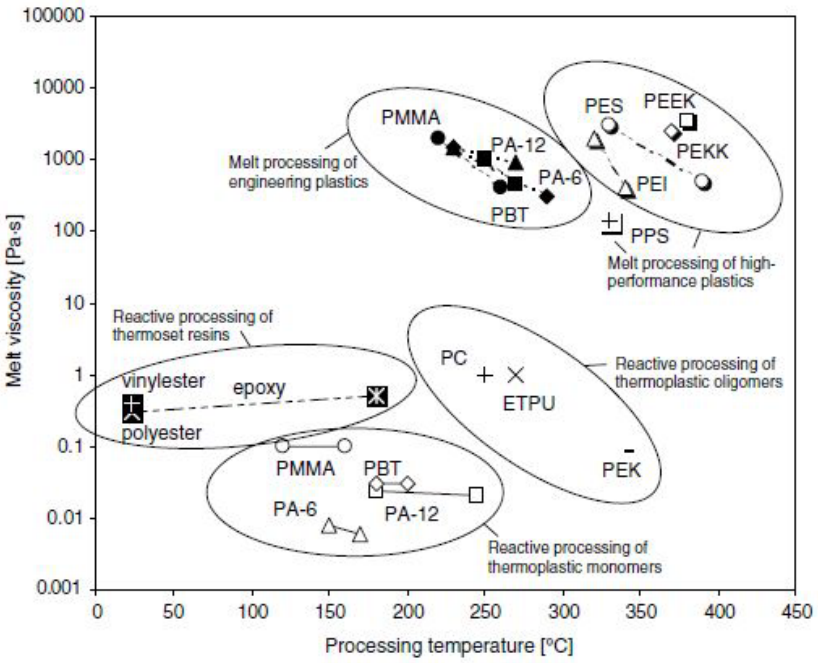

Figure 1. 3 Melt viscosities and processing temperature of various matrix materials for both reactive and melt processing (Reproduces from [6])

As seen in Figure 1. 3 and Table 1. 1, there are several kinds of monomers have low viscosities below 1 Pa·s, which is suitable for liquid molding process. However, processing temperatures of most monomers such as polyamide-12 (PA-12), polyethyleneteraphthalate (PET), polybutyleneteraphthalate (PBT) and polycarbonate (PC) are too high (above 200℃) for T-RTM process. Although processing temperature of polymethylenethacrylate (PMMA) is below 200℃, its processing time is too long at low temperature, while its monomer is easily boiling at high temperature which causes void in composites. Therefore, polyamide-6 (PA6) monomer, which called ε-caprolactam, is the most promising material among these thermoplastic precursors [6-8].

Table 1. 1 Processing temperatures and processing times of various monomers

Monomer	Processing temp.	Processing time
PMMA	120-160℃	@low temp.: > 16 hrs @high temp.: Boiling of monomer ⇒ void
PA-6	130-170℃	3-60 mins
PA-12	180-240℃	with cooling process
PET	250-325℃	3-15 mins
PBT	180-200℃	< 30 mins
PC	240-280℃	2-5 mins

Overall, the performance of automotive parts using CFRP composites are improving and the cycle time is decreasing within 5 minutes [2, 6]. In addition, the studies on the development of low cost carbon fiber is also steadily progressing (Figure 1. 4), which leads to a lower cost of automotive parts with CFRP composites.

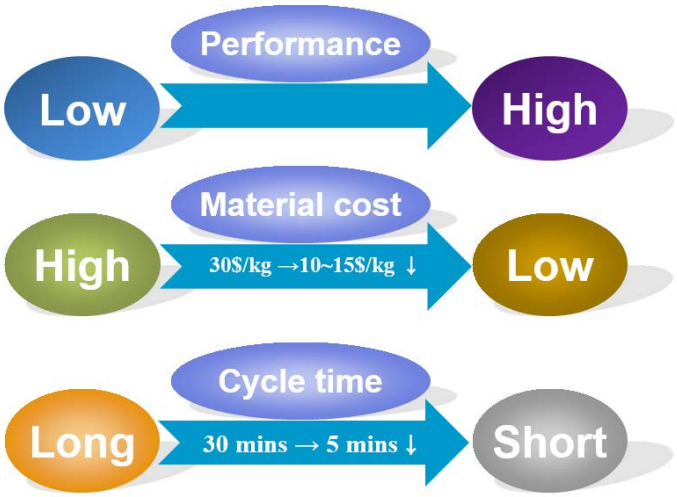

Figure 1. 4 Development tendency of performance, price, and cycle time of CFRP composites for automotive parts

1.2 Literature review

Carbon fiber reinforced plastic (CFRP) composites have been widely used in place of metallic materials, and one of the popular carbon fiber reinforced thermoplastic (CFRTP) composites is ε-caprolactam based CFRTP composites due to its watery viscosity and fast polymerization time.

For resin transfer molding (RTM) process, polymerization kinetics plays a key role to the properties of products, and the main factors which affect polymerization kinetics are shown as Figure 1. 5. Researches on in situ polymerization of ε-caprolactam have already been carried out. Ahmadi et al. suggested that the correct ratio of monomer, catalyst and activator is a key component of the anionic ε-caprolactam polymerization, which leads to the least monomer residue and the best properties of PA6 samples [9-11]. In addition, various types of catalyst and activator had been used for anionic polymerization of ε-caprolactam to investigate polymerization rate, monomer conversion, mechanical properties, electrical conductivity, and so on [12-17]. Using these polymerization techniques, Gong et al. fabricated polyamide single polymer composites via resin transfer molding; however, the reaction time is too long for automotive industry [18, 19].

Numerous studies on polymerization of ε-caprolactam have been performed using various types and ratios of catalyst and activator. Only a few studies, however, have been conducted on ε-caprolactam based CFRTP composites using

RTM process within several minutes in order to reduce the cycle time of molding processes.

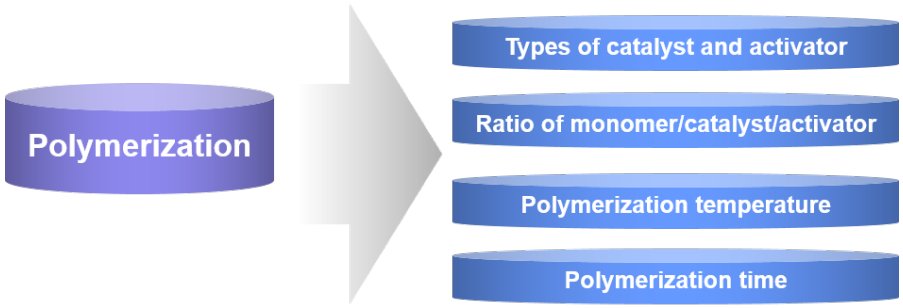

Figure 1. 5 Factors that affect polymerization kinetics

Since the polymerization of ε-caprolactam occurs rapidly in the presence of the catalyst and activator, A pallets (caprolactam & activator) and B pallets (caprolactam & catalyst) are sold separately in order to prevent the mold from being completely injected during the injection process. As shown in Figure 1. 6, A pallets and B pallets provided in the market are solid states; therefore, it is necessary to keep two kinds of mixtures in the melt state before mixing. The reaction tanks are separated into two parts in order to prevent polymerization of ε-caprolactam, which start to polymerize in the mixing zone and may obstruct resin flow to the mold. Thus, it is important to choose proper temperatures of two tanks and mold.

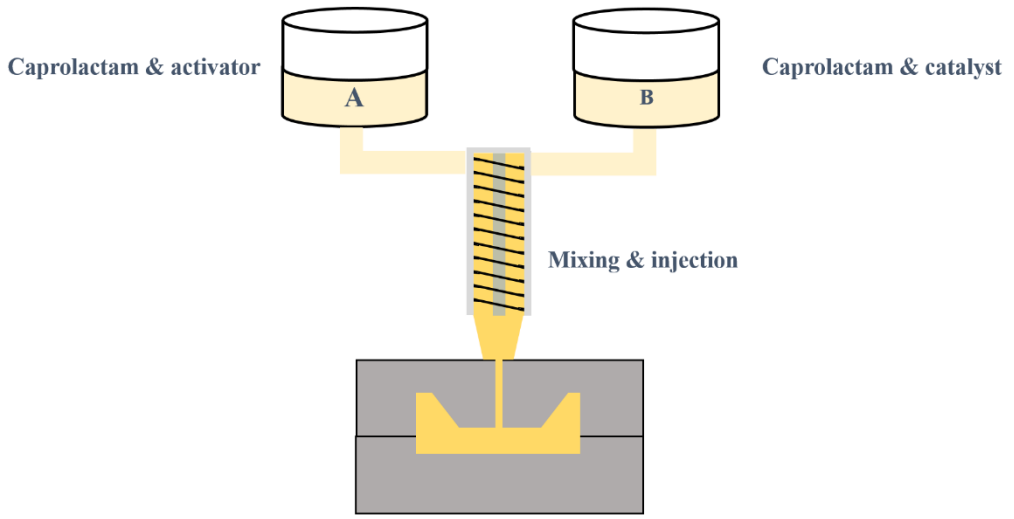

Figure 1. 6 Schematic illustration of T-RTM

Recently, Ben et al. studied glass fiber reinforced thermoplastic (GFRTP) composites and CFRTP composites with A (caprolactam & activator) mixtures and B (caprolactam & catalyst) mixtures to evaluate their mechanical properties [20, 21]. However, few studies on polymerization kinetics and modeling related to experimental has been carried out. Considering large scale products, polymerization kinetics must be studied to control molding processes and cycle time.

1.3 Objective of research

As mentioned above, reduction of cycle time is a key issue for automotive industry and the cycle time is significantly affected by the polymerization kinetics. Therefore, polymerization kinetics is very crucial for the whole molding process. There are some parameters which can influence polymerization kinetics, such as types of catalyst and activator, ratio of catalyst and activator, molding temperature, and so on.

In this study, we focused on the effect of molding temperature on the mechanical properties and polymerization kinetics (Figure 1. 7). Meanwhile, heating rate plays an important role in polymerization and crystallization kinetics, which can directly affect the mechanical properties of pure PA6 and CFRTP composites. In order to approach this objective, the following sub-objectives should be conducted.

- Conducting the mechanical properties of pure PA6 and CFRTP composites at various molding temperatures.
- Evaluating the relationship between crystallinity of pure PA6 or CFRTP composites and molding temperatures.
- Evaluating the effect of heating rate on the polymerization and crystallization kinetics.

- Separating crystallization and polymerization curves during heating process.
- Modeling the relationship between temperature and polymerization and crystallization kinetics.
- Comparing experimental and numerical simulation results in order to analyze large scale automotive parts with various shapes and sizes.

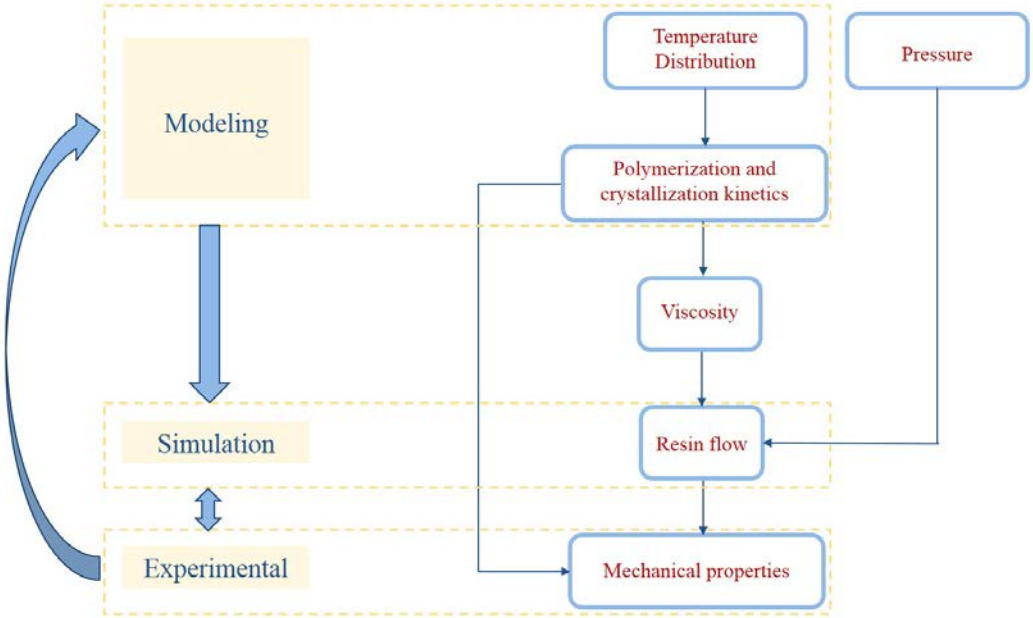

Figure 1. 7 Research objective

1.4 Outline of dissertation

Chapter 2 describes overall experimental setting and process, materials, and characterization methods for polymerization kinetics and mechanical properties. Furthermore, the mechanical properties of PA6 and CFRTP composites are discussed in terms of various molding temperatures in Chapter 3. Chapter 4 deals with the method to separate polymerization peaks, and also focuses on modeling of dynamic scanning and isothermal scanning process of PA 6, which is important data for further simulation. Finally, numerical simulation presents in Chapter 5. Simulation results are compared to experimental results to verify the accuracy of the modeling data that can be used to analyze large scale automotive parts with various shapes and sizes.

CHAPTER 2. Materials and Process

Thermoplastic composites have gained steady favor over traditional materials due to their specific strength, recyclability and impact resistance. Thus, the use of such materials in structural applications can be expanded especially in automotive industry. Recently, three main types of fiber reinforced thermoplastic composites used for interior and exterior parts have been studied, such as natural fiber reinforced thermoplastic (NFRTP) composites [22-24], glass fiber reinforced thermoplastic (GFRTP) composites [25-27] and carbon fiber reinforced thermoplastic (CFRTP) composites [28-30].

Considering environmental issues, it is most desirable to manufacture automotive parts using NFRTP composites; however, natural fibers are susceptible to high molding temperature and have a high water absorption, which can reduce mechanical properties of the products. Therefore, among these reinforcements, CFRTP composites are widely used in the automotive industry due to high mechanical properties of carbon fiber.

Generally, thermoplastic polymer have high viscosity in spite of high temperature. Therefore, manufacturing method of thermoplastic composites have been limited to extrusion, injection molding, compression molding, and so on

(Figure 2. 1). However, it needs high processing temperature and pressure which may cause high cost of products. Moreover, some techniques are incompatible with continuous woven fabrics or long fibers, which can affect the mechanical properties of composites.

Therefore, there has been an increasing interest in liquid molding of thermoplastic resin composites using monomer which is a molecule that may bind chemically or supramolecularly to other molecules to form a polymer. Generally, a monomer has low viscosity even at a low temperature, which means that its composites can be made via the manufacturing techniques that are applied for thermosetting resin composites, such as resin transfer molding (RTM). The monomers can be polymerized during liquid molding process, so processing time can be reduced compared to thermosetting resin that need curing time. In order to prepare high volume fraction carbon fabric reinforced thermoplastic composites, vacuum assisted resin transfer molding (VaRTM) technique was used in this study. VaRTM is similar to RTM, but because the catalyst is sensitive to moisture during the experiment, the environment in tank and mold was kept vacuum during mixing and injection.

In this chapter, materials and experimental setting and processes will be presented.

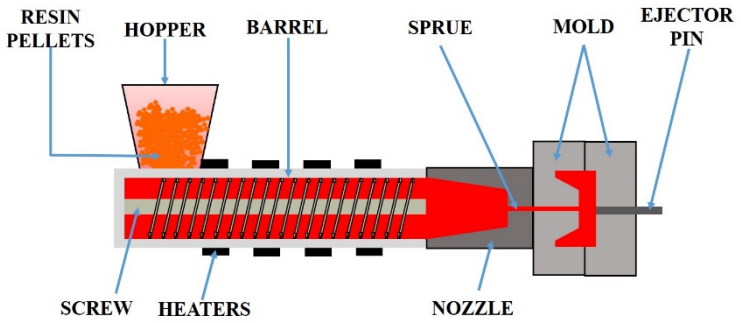

(a) Injection molding

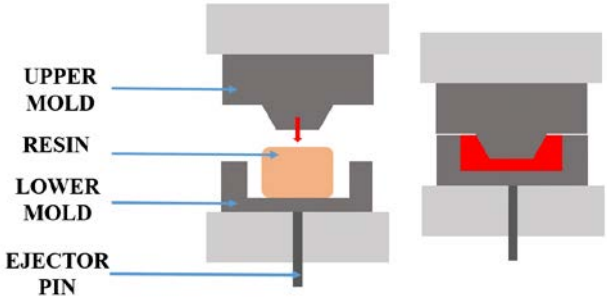

(b) Compression molding

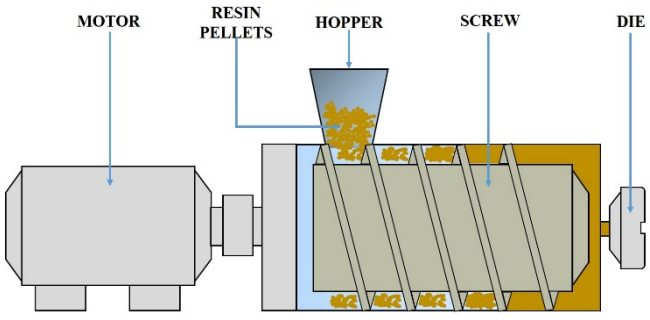

(c) Extruder

Figure 2. 1 Schematic illustration of the manufacturing process for thermoplastic resin

2.1 Materials

2.1.1 Monomer

A monomer is a molecule that may bind chemically or supramolecularly to other molecules to form a polymer. The process by which monomers combine end to form a polymer is called polymerization [31].

ε-Caprolactam is a monomer with ring structure (Figure 2. 2), and it is the precursor to nylon 6 which is widely used as synthetic polymer. ε-Caprolactam was first described in the late 1800s when it was prepared by the cyclization of ε-aminocaproic acid, the product of the hydrolysis of caprolactam [32].

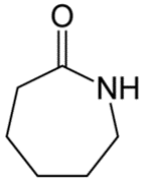

Figure 2. 2 Formula of ε-caprolactam

Compared to epoxy resin, ε-caprolactam has watery viscosity at 110℃, which is just about three or four times that of water (Table 2. 1). Therefore, it is much easier to inject ε-caprolactam resin to the mold than thermoset resin like epoxy.

Table 2. 1 Viscosity of polymers at a specified temperature

Item	Viscosity (mPa·s)
ε-Caprolactam (110 °C)	3 - 4
Epoxy (25°C)	800
Fast curable epoxy (60°C)	130

In this study, ε-caprolactam (DSM, Netherlands) was used as monomer, and it was mixed with catalyst and activator for anionic polymerization at specified molding temperatures.

2.1.2 Catalyst and activator

Anionic polymerization of ε-caprolactam to form nylon-6 is well known as Figure 2. 3. The anionic polymerization of caprolactam can be controlled by the types of catalyst and activator or the ratio of catalyst and activator.

In this study sodium metal (DAEJUNG, Korea) and hexamethylene diisocynate (HMDI) (Wako, Japan) were used as a catalyst and activator, respectively.

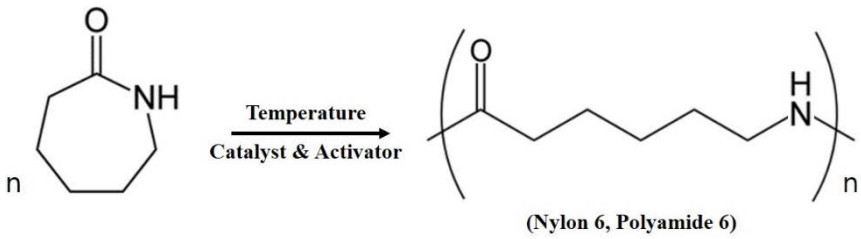

Figure 2. 3 Anionic polymerization of ε-caprolactam

2.1.3 Reinforcement

As mentioned above, natural fiber reinforcement [33-35], glass fiber reinforcement [36, 37] and carbon fiber reinforcement [38, 39] are usually used for automotive parts. Carbon fiber reinforced composites have a lower density compared to glass fiber reinforced composites with the same weight percent per cubic meter. In addition, among these reinforcements, carbon fiber are much stronger and stiffer than others per unit of weight. Especially, continuous carbon fabrics reinforced composites have better physical properties than short carbon fiber reinforced composites.

In this study, plain carbon fabric (MUHAN COMPOSITES, Korea) (Figure 2. 4) was used as a reinforcement with thickness of 0.22mm, and the specification is shown as Table 2. 2.

Figure 2. 4 Carbon fabric used in this study

Table 2. 2 Specification of carbon fabric

Product	Weaving Methods	Width (mm)	Wrap	Fill	Weight (g/m^2)
C-120	Plain	1000/1500	Carbon 3K	Carbon 3K	200

2.2 Setting and process

Vacuum assisted resin transfer molding (VaRTM) has been very developed and is now a proven low-cost manufacturing technique for thermosetting resin composites. The resin suitable for VaRTM techniques must have a low viscosity (< 1 Pa·s) during resin transfer molding process. However, it takes a long cycle time for thermosetting resins including curing time and cooling time, and it is difficult to repair and recycle. To overcome these problems of thermosetting based composites, thermoplastics composites have been received a lot of attention.

ε-Caprolactam, which is a monomer of thermoplastic polymer named polyamide 6 (PA6), has much lower viscosity than that of traditional epoxy and fast curable epoxy. Therefore, it a good option to use VaRTM techniques for ε-caprolactam resin based composites.

2.2.1 Experimental setting

Figure 2. 5 shows the experimental setting of VaRTM process. Monomer and catalyst were melted in the oil bath, and 13 layers of carbon fabric were piled in the mold before molding.

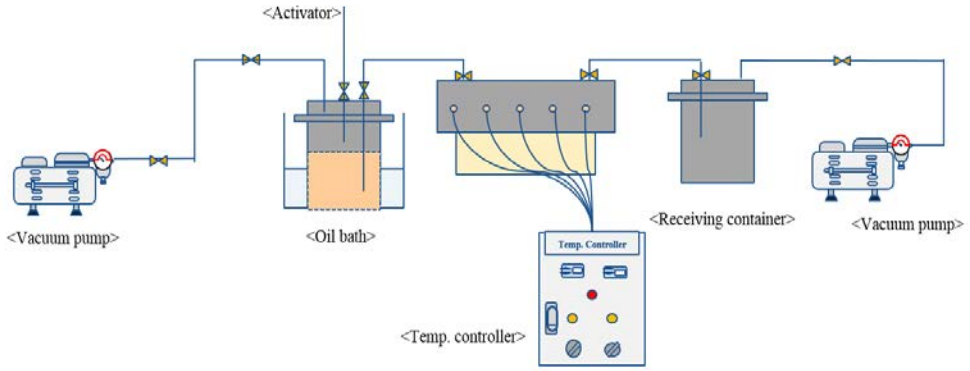

Figure 2. 5 Schematic illustration of the VaRTM process

The catalyst for the anionic polymerization of ε-caprolactam is sensitive for humidity in the air, so the container in the oil bath keep the vacuum condition during the melting process and the mold must be sealed well. The lower mold was designed as Figure 2. 6. The runner of the lower mold is to let the resin be uniformly injected into the carbon fabrics from outside to inside.

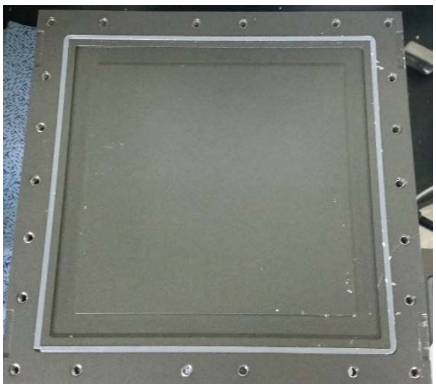

Figure 2. 6 Design for lower mold

2.2.2 Experimental process

The catalyst for the anionic polymerization of ε-caprolactam is sensitive for humidity in the air; therefore, all the materials used in this study must be fully dried in order to prevent moisture from interfering with the polymerization process.

ε-Caprolactam was dried at 40℃ for 24 hours with silica gel blue in vacuum oven. Meanwhile, carbon fabric was washed with acetone to remove binding agent, which may decrease the interfacial performance between resin and fiber, before the installation into the lower mold, and it was also dried at 80℃ for 5 minutes to remove the moisture. A pre-specified ratio of ε-caprolactam and sodium metal were melted at 110℃ for 1 hour with vacuum condition. The dried carbon fabric was piled in the mold and sealed the mold well before injection.

After melting, activator was injected to the mixture of monomer and catalyst, and then transferred to the mold heated for 5 minutes for polymerization. The temperature of mold was set at 120℃, 140℃, 160℃, 180℃ and 200℃, respectively. Finally, the specimen was released from the mold without cooling (Figure 2. 7).

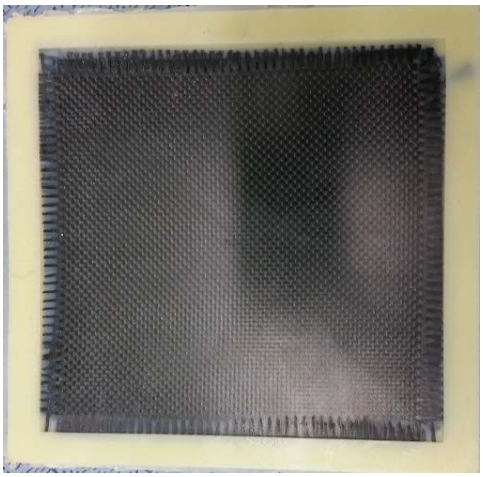

Figure 2. 7 Photographs of fabricated CFRTP composites

2.3 Characterization methods

2.3.1 Mechanical properties

In order to investigate mechanical properties of pure PA6 and CFRTP samples, the following tests were conducted.

First, content of unreacted monomer was measured to evaluate the degree of polymerization at different molding temperatures. Furthermore, content of water absorption, which may affect mechanical properties of products, was also measured.

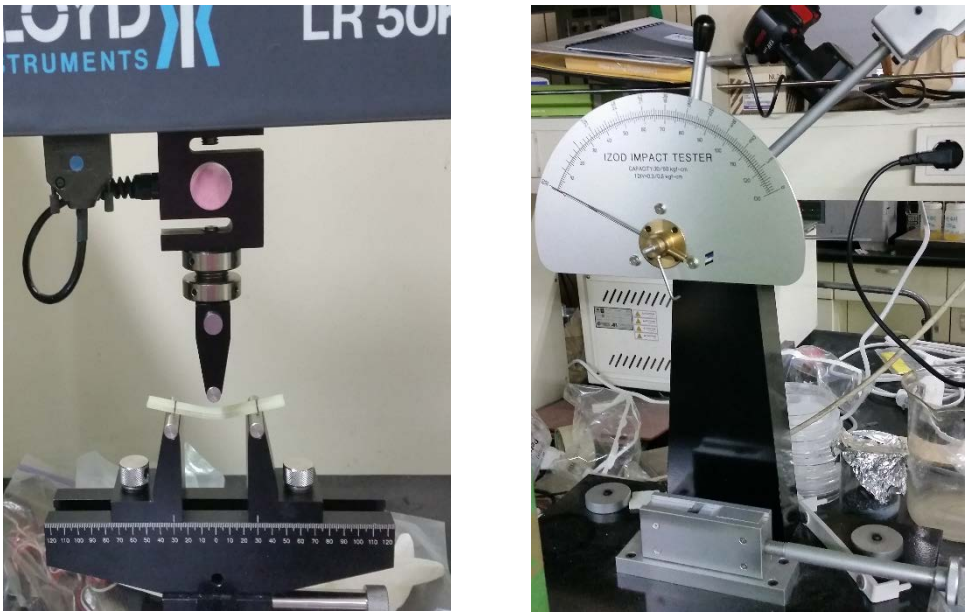

Figure 2. 8 Device for three point bending test and izod impact test

In terms of automotive parts, flexural strength, flexural modulus and impact strength are important properties. Therefore, three point bending tests and izod impact tests were carried out for the samples molded at different molding temperatures. Instron-5584 (Instron, UK) universal materials testing machine and Izod impact tester (SALT, Korea) were used to measure bending properties and impact properties of pure PA6 and CFRTP composites (Figure 2. 8). The methods and results for these mechanical tests are described in detail in Chapter 3 below.

2.3.2 Differential scanning calorimetry (DSC) analysis

Differential scanning calorimetry (DSC) analysis is a thermos analytical technique in which the difference in the amount of heat required to increase the temperature of a sample and reference are measured as a function of temperature (Figure 2. 9). Both the sample and reference are maintained at nearly the same temperature throughout the experiment. Generally, the temperature program for a DSC analysis is designed such that the sample holder temperature increases linearly as a function of time. The reference sample should have a well-defined heat capacity over the range of temperatures to be scanned.

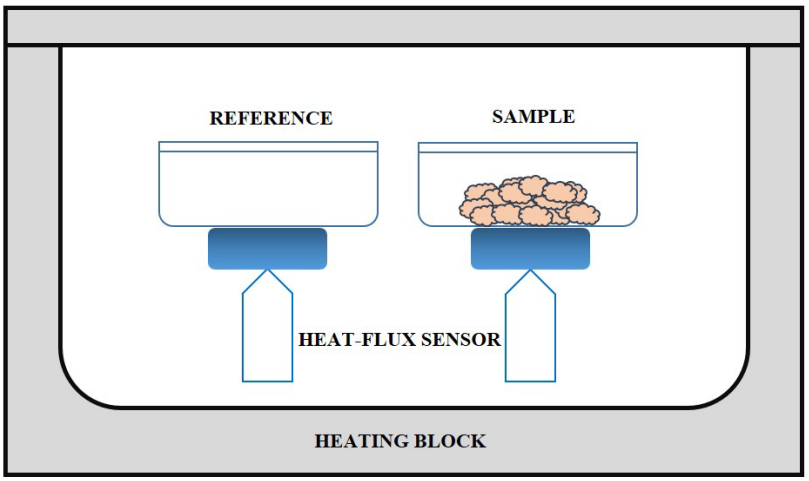

Figure 2. 9 Schematic illustration of differential scanning calorimetry

The basic principle underlying this technique is that, when the sample undergoes a physical transformation such as phase transitions, more or less heat will need to flow to it than the reference to maintain both at the same temperature. Whether less or more heat must flow to the sample depends on whether the process is exothermic or endothermic. For example, as a solid sample melts to a liquid it will require more heat flowing to the sample to increase its temperature at the same rate as the reference. This is due to the absorption of heat by the sample as it undergoes the endothermic phase transition from solid to liquid. Likewise, as the sample undergoes exothermic processes less heat is required to raise the sample temperature. By observing the difference in heat flow between the sample and reference, DSCs are able to measure the amount of heat absorbed or released during such transitions. DSC can also be used to observe more subtle phase changes, such as glass transitions.

Since the heat evolution dH/dt can be measured by the DSC results from the polymerization reaction, it is possible to relate the heat evolution (dH/dt) to the rate of conversion (dα/dt) and the conversion (α) according to the following two equations (Eq.s (2.1) & Eq.s (2.2)).

$$\frac{d\alpha}{dt} = \frac{1}{\Delta H_{tot}} \left(\frac{dH}{dt}\right)_t \qquad \textbf{(2.1)}$$

$$\alpha = \frac{1}{\Delta H_{tot}} \int_{t_0}^{t} \left(\frac{dH}{dt}\right)_t \, dt \qquad \textbf{(2.2)}$$

Where $\triangle H_{tot}$ is the total heat of reaction, generally determined by averaging the reaction exotherms measured from several dynamic temperature DSC runs. Various chemical kinetic models can then be fit using data which is obtained from isothermal DSC experiments. The modeling section is discussed in detail in Chapter 4, and the data related to the conversion and time will be used in Chapter 5 to predict the viscosity change with the polymerization time, which was used for simulation analysis.

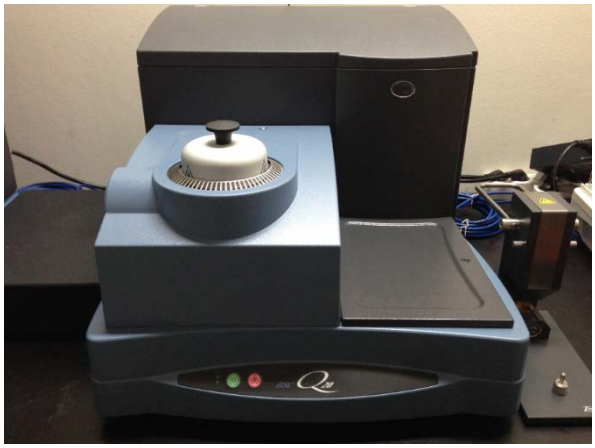

Figure 2. 10 Differential scanning calorimetry (DSC) device

In this study, DSC (Q20, TA Instruments) was used to observe polymerization kinetics of ε-caprolactam during both dynamic and isothermal scanning process (Figure 2. 10).

CHAPTER 3. Mechanical properties

3.1 Measurement of unreacted monomer and water absorption

After polymerization, there still exists a certain amount of unreacted monomer, which is very hydroscopic and is readily dissolved in water. In order to check the conversion of ε-caprolactam, unreacted monomer and water absorption test was conducted.

The sample size is 60mm x 10mm x 3.75mm, and the results shown in Figure 3. 1 and Figure 3. 2 are the average data of five samples in each case. Each sample was dried at 60 ℃ for 24 hours in a depressurized chamber, and its weight was measured and marked as W_0. After that, each was put in hot water at 80 ℃ for 72 hours, and its weight was signed as W_2. Finally, each sample was dried at 60 ℃ for 72 hours in a vacuum chamber again, and its weight recorded as W_1.

With these data, we can obtain the content of unreacted monomer and water absorption of PA6 and CFRTP composites using Eqs. (3.1) and Eqs. (3.2).

$$W_u = \frac{W_0 - W_1}{W_0} \times 100\% \quad \textbf{(3.1)}$$

$$W_a = \frac{W_2 - W_1}{W_2} \times 100\% \quad \textbf{(3.2)}$$

Where W_u is content of unreacted monomer and W_a is content of water absorption.

Figure 3. 1 shows the percentage of the unreacted monomer (W_u) of PA6 and CFRTP composites. It can be seen that the content of unreacted monomer for both pure PA6 and CFRTP composites shows lowest value at 140℃.

Figure 3. 2 represents the content of water absorption (W_a) of pure PA6 and CFRTP composites. It has the same tendency with the content of unreacted monomer. Both pure PA6 and CFRTP composites show the lowest content of water absorption value at 140℃.

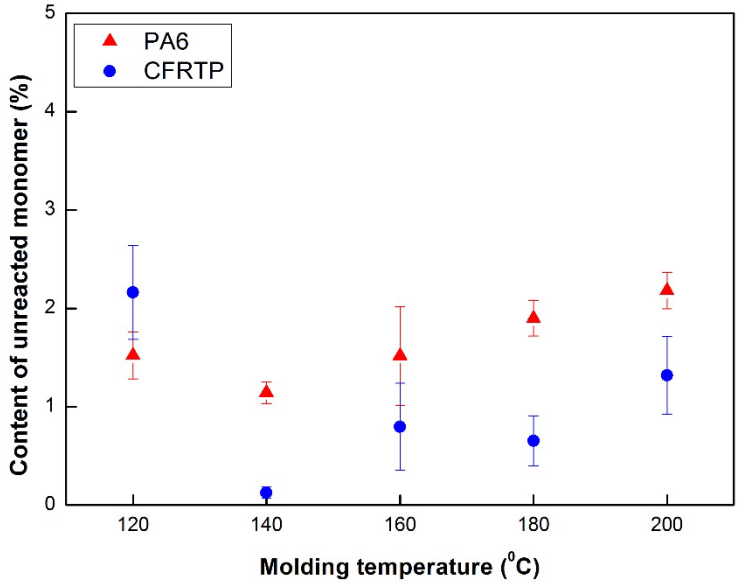

Figure 3. 1 Content of unreacted monomer of pure PA6 and CFRTP composites

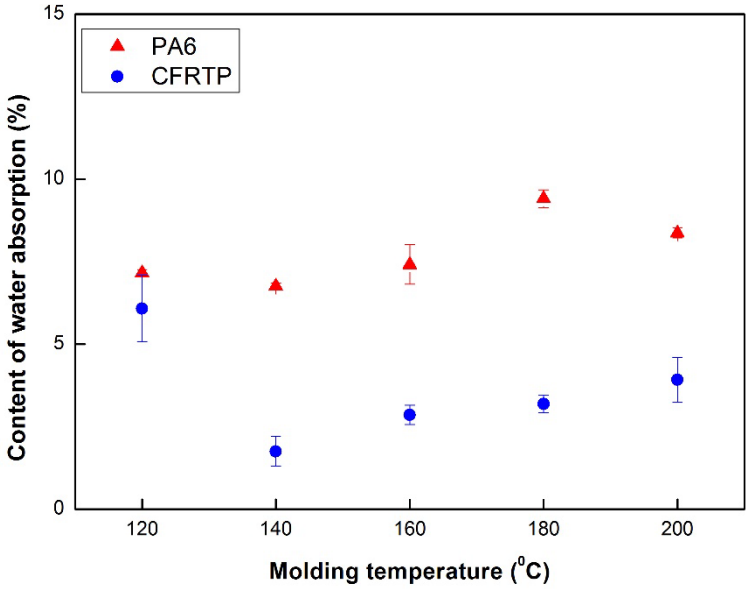

Figure 3. 2 Content of water absorption of pure PA6 and CFRTP composites

In addition, both the contents of unreacted monomer and water absorption increased with the increasing molding temperature. From the results, we can refer that there is an optimum temperature for polymerization of ε-caprolactam, and the optimum temperature may exist between 140℃ and 160℃.

Furthermore, both the contents of unreacted monomer and water absorption of pure PA6 and CFRTP have a similar tendency, which may indicate that the carbon fabrics which used as reinforcement rarely affect the polymerization of ε-caprolactam.

3.2 Three point bending test

Bending properties are very critical for CFRTP composites used for automotive products. In order to obtain the bending strength and bending modulus, each specimen was cut to 100mm x 13mm x 3.75mm according to ASTM D790-10. The span length was 60 mm, and nine specimens were tested for each case.

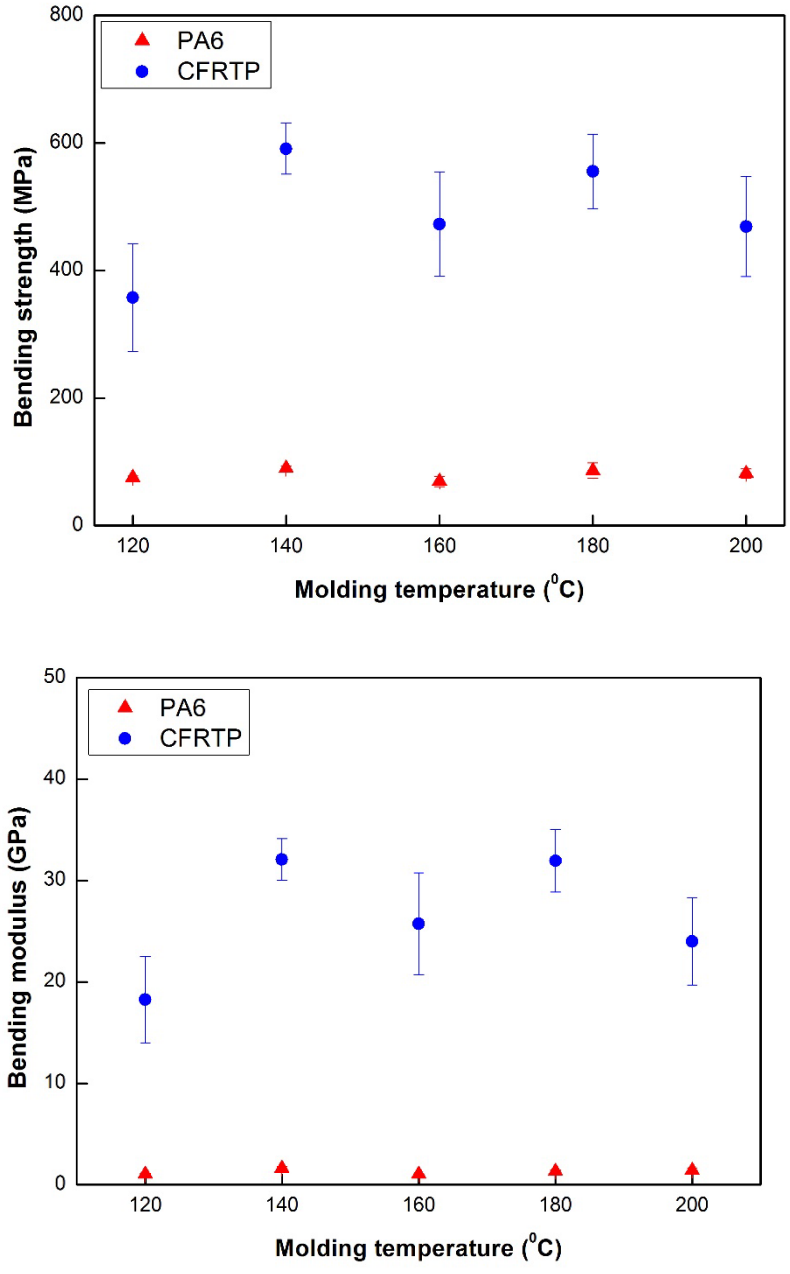

Figure 3. 3 Bending strength and modulus of pure PA6 and CFRTP at different molding temperatures

Figure 3. 3 show the bending results of pure PA6 and CFRTP composites. It shows the highest value of the bending strength and bending modulus at 140℃, at which the content of unreacted monomer and water absorption is the lowest. It seems to be correlated to the results above.

3.3 Izod impact test

The Izod impact test was performed based on ASTM D256 in order to evaluate the impact resistance of the specimen in each case. Each specimen had a dimension of 61.5mm in height, 11.5mm in depth, 3.75mm in width and 2.54mm in a notch depth. Eleven specimens were tested for each case.

It can be seen that impact strength of pure PA6 molded at 120℃ and 200℃ is lower than that of other samples due to unreacted monomer (Figure 3. 4). However, Figure 3. 5 shows that impact strength of the CFRTP composites, which were molded at 120℃ and 200℃, shows much higher values than those of others. It may be that impregnation of carbon fibers at 120℃ and 200℃ is worse than that of others, and there is much unreacted monomer when it was molded at 120℃ and 200℃. Specimens of CFRTP-120 and CFRTP-200 showed

the partial break mode, while the others showed completely break mode. It can further confirm the reason why the impact strength of CFRTP-120 and CFRTP-200 show higher values than those of other specimens.

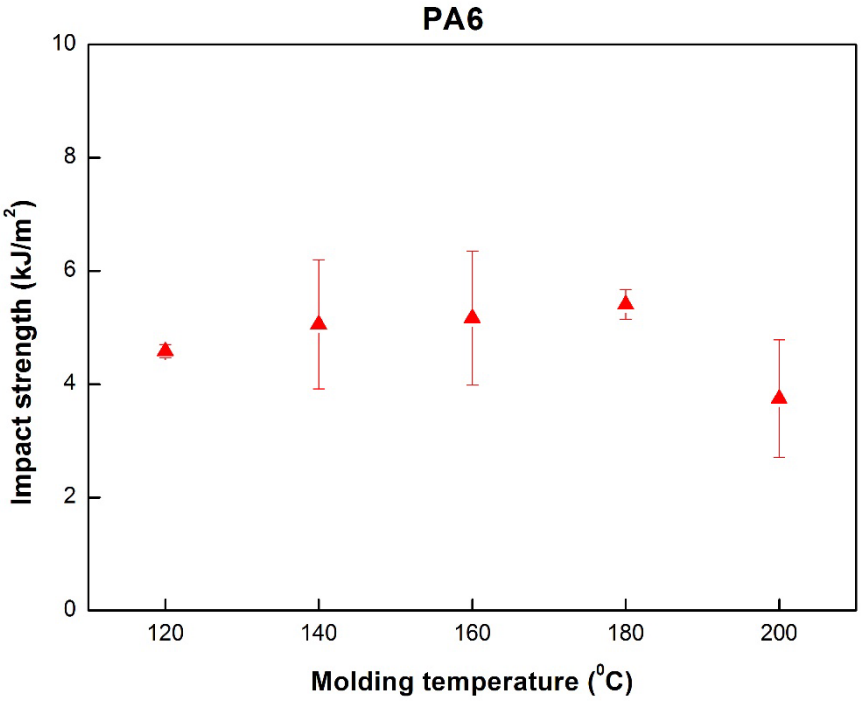

Figure 3. 4 Impact strength of pure PA6 at different molding temperatures

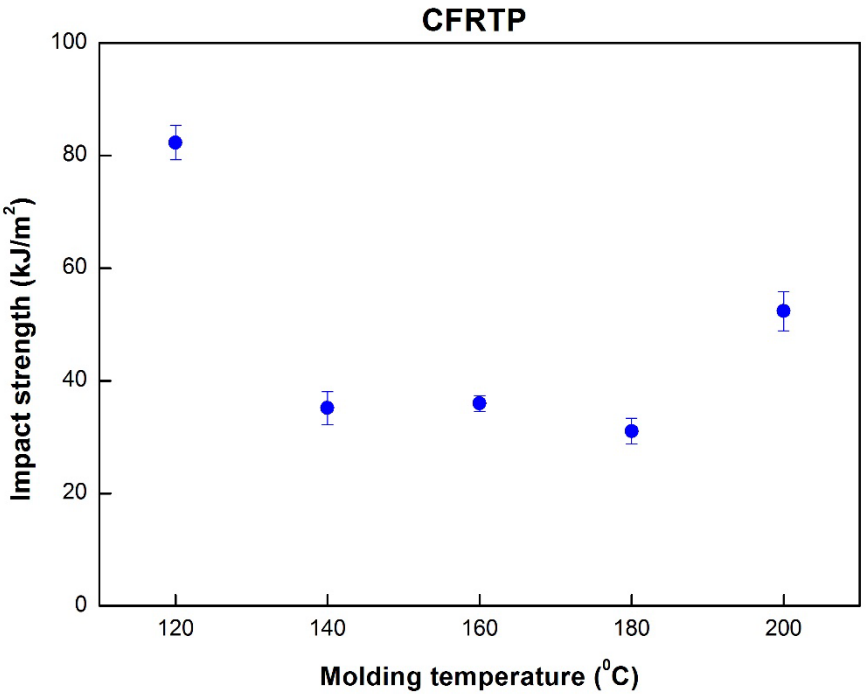

Figure 3. 5 Impact strength of CFRTP at different molding temperatures

3.4 Scanning electron microscope (SEM) observation

In order to evaluate the adhesion between the fibers and the resin, the fracture surface of the CFRTP specimen molded at different molding temperatures were observed with a scanning electron microscope.

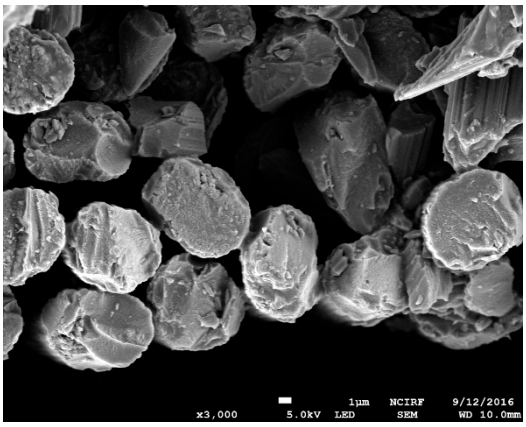
x3,000 5.0kV LED 1µm NCIRF SEM 9/12/2016 WD 10.0mm

(a)

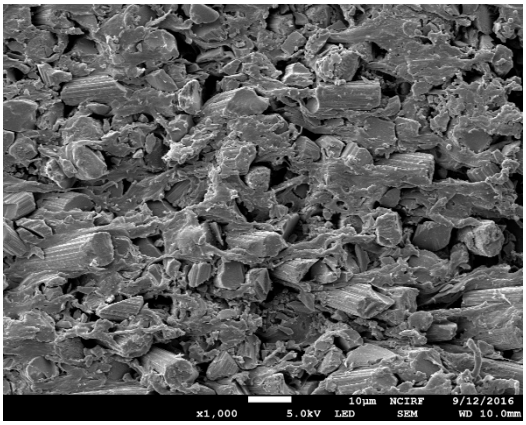
x1,000 5.0kV LED 10µm NCIRF SEM 9/12/2016 WD 10.0mm

(b)

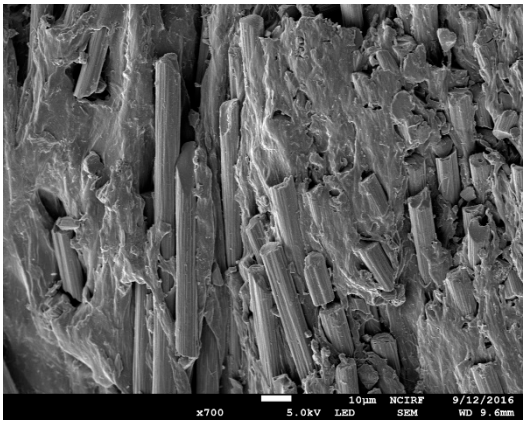
x700 5.0kV LED 10µm NCIRF SEM 9/12/2016 WD 9.6mm

(c)

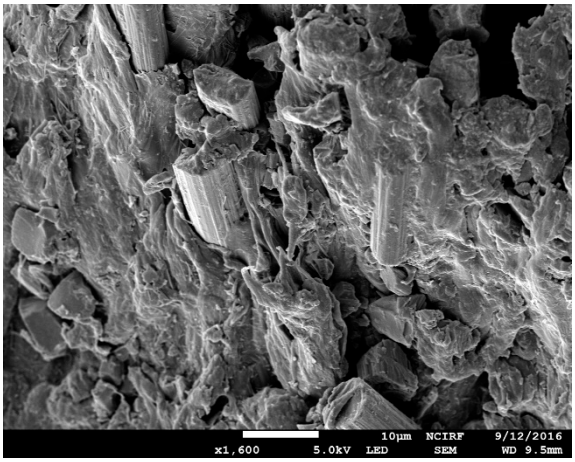

(d)

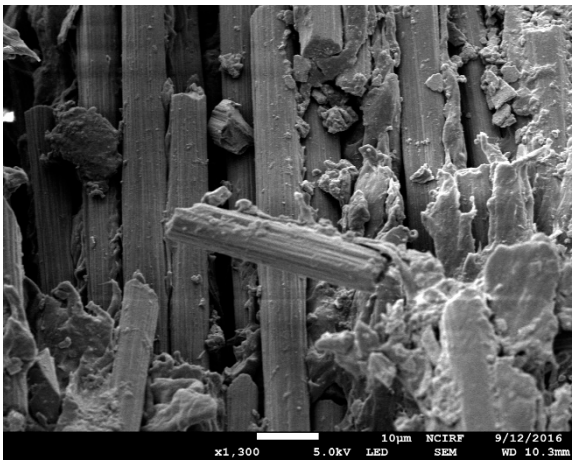

(e)

Figure 3. 6 SEM micrograph of the fracture surface of CFRTP at different molding temperatures. (a) 120℃, (b) 140℃, (c) 160℃, (d) 180℃, and (e) 200℃

Figure 3. 6 (a) to (e) represent that the resin is homogenously impregnated around the carbon fabrics which were molded at 140℃, 160℃ and 180℃. However, there is much resin around the carbon fabrics which were molded at 120℃ and 200℃ due to unreacted monomer. The results are correlated to the mechanical properties of the specimens each case.

3.5 Crystallinity of CFRTP composites

In order to evaluate the crystallinity during the molding process, differential scanning calorimetry (DSC) was performed (i.e. about 10mg each sample). As in Figure 3. 7, the endothermic peak occurs at a temperature above 200℃, which can be considered as the energy related to crystallinity in samples. The crystallinity of each sample was calculated by dividing the heat of fusion ($\triangle H_m$) of each sample by 190 J/g, which is the heat of fusion of 100% crystalline PA6 (Eq.s (3.3) & Eq.s (3.4)).

$$\text{Degree of crystallinity} = (\Delta H_m / \Delta H_m^{100\%}) \times 100\% \quad \textbf{(3.3)}$$

$$\Delta H_m^{100\%} = 190\, J/g \quad \textbf{(3.4)}$$

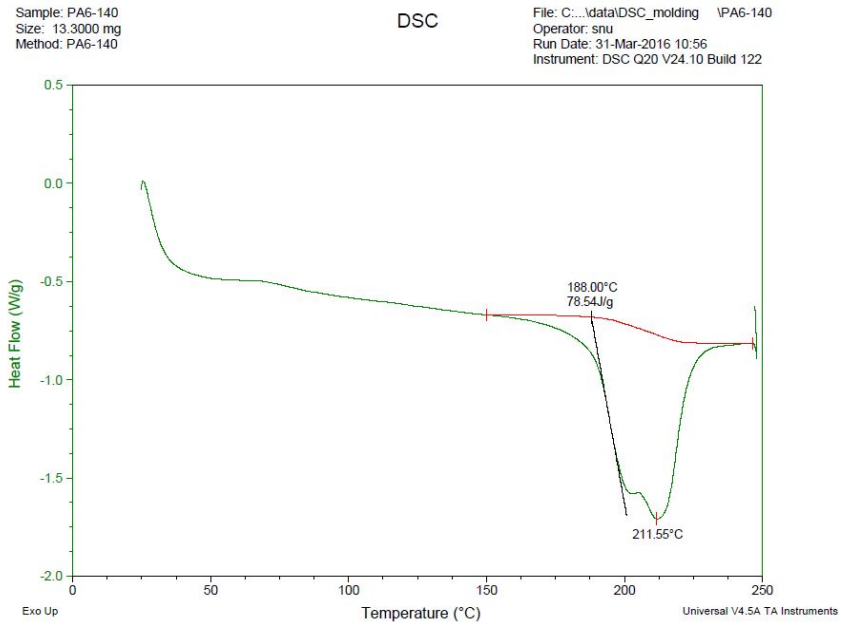

Figure 3. 7 DSC thermograms of the molded samples

Table 3. 1 Degree of crystallinity for pure PA6 and CFRTP composites at different molding temperatures

Molding temperature (℃)	PA6		CFRTP	
	Heat of fusion (J/g)	Crystallinity (%)	Heat of fusion (J/g)	Crystallinity (%)
120℃	88.25	46.45	105.39	55.47
140℃	78.54	41.35	86.84	45.70
160℃	76.05	40.03	79.43	41.81
180℃	69.85	36.76	75.65	39.82
200℃	67.83	35.70	66.32	34.91

Table 3. 1 and Figure 3. 8 shows the degree of crystallinity which was affected by a specified molding temperature for pure PA6 and CFRTP composites. It can be seen that crystallinity of both pure PA6 and CFRTP composites decreased as the molding temperature increases. In addition, the degree of crystallinity of CFRTP is higher than that of PA6 because carbon fabric may act as nucleation agents.

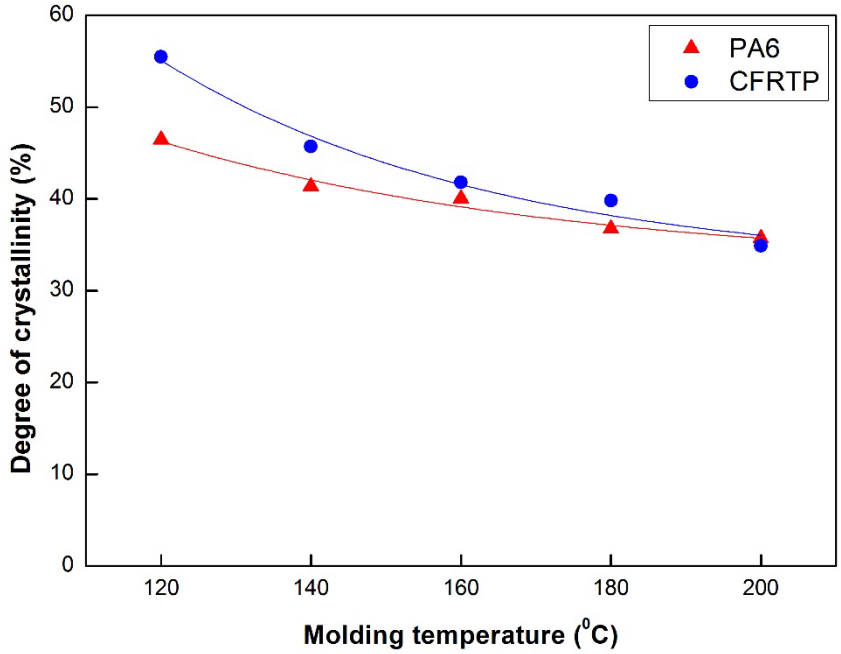

Figure 3. 8 Degree of crystallinity for pure PA6 and CFRTP composites at different molding temperatures

According to results from all of the mechanical properties, we can conclude that the optimum molding temperature for polymerization is between 140℃ and 160℃.

CHAPTER 4. Investigation of polymerization kinetics

The degree of polymerization and crystallinity are the factors that greatly affect the mechanical properties of the samples. Meanwhile, these two factors occurs simultaneously, thus it is difficult to carry out the study on polymerization behavior only. In this chapter, we focused on the polymerization kinetics by temperature distributions.

In order to study the relationship between temperature and polymerization, Differential scanning calorimetry (DSC) was conducted for both dynamic scanning and isothermal scanning process.

DSC samples were prepared by the following steps:

First, ε-caprolactam was dried at 40℃ for 24 hours with silica gel blue in vacuum oven to remove moisture. Subsequently, dried ε-caprolactam and sodium metal were melted at 110℃ in the oil bath for 1 hour under vacuum condition. After that ε-caprolactam and sodium metal mixture was cooled to 70℃

following by the addition of activator, and the mixture was transferred to a glass vial and sealed. Finally, this sealed vial was rapidly cooled in the liquid nitrogen and taken to the DSC pan (i.e. about 10mg each). These samples were used for both dynamic scanning and isothermal scanning process.

4.1 Dynamic scanning

4.1.1 Analysis of polymerization kinetics at different heating rates

DSC samples were heated from room temperature to 250℃ at a heating rate of 10℃/min, 15℃/min, 20℃/min, 30℃/min and 50℃/min. In Figure 4. 1, the first peak corresponds to melting of ε-caprolactam at around 70℃, and the second peak shows polymerization and crystallization peak during heating process. In this process, polymerization and crystallization occurs simultaneous, and both are exothermic processes. The third peak means melting of PA6, which is related to the crystallization during the heating process.

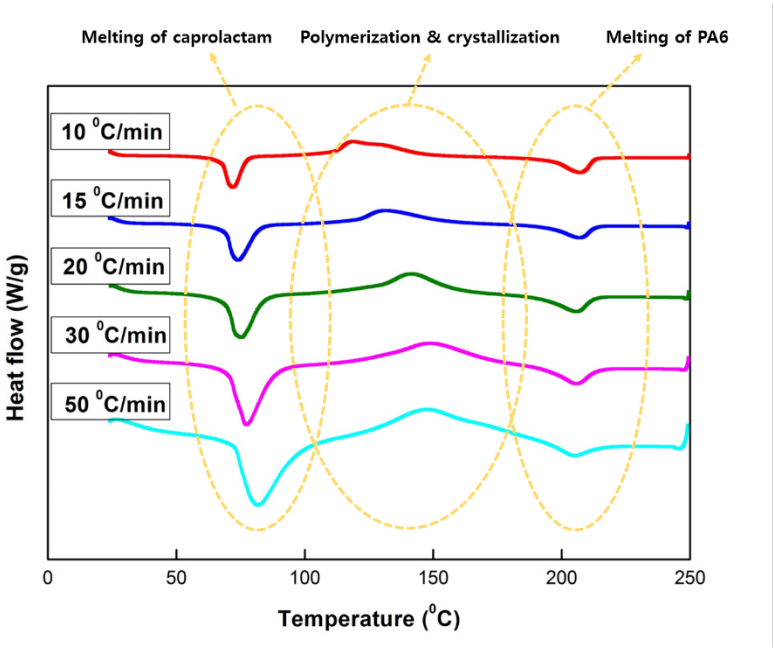

Figure 4. 1 DSC thermograms of caprolactam at five different heating rates

Table 4. 1 The values of heat of fusion during heating process

Heating rate (℃/min)	Melting of caprolactam	Polymerization & crystallization	Melting of PA6		Polymerization
	Heat of fusion (J/g)	Heat of fusion (J/g)	Heat of fusion (J/g)	Crystallinity (%)	Heat of fusion (J/g)
10	113.37	147.60	77.65	41.00	69.95
15	114.33	137.16	64.81	34.25	72.35
20	119.53	136.60	63.92	33.79	72.68
30	119.70	106.22	32.12	17.44	74.10
50	124.27	90.34	12.15	6.48	78.19

According to the second and third peak, we can calculate heat of fusion of crystallization and polymerization respectively. It can be seen in Figure 4. 2, crystallinity simultaneous with polymerization was decreased by increasing the heating rate. The reason may be that synthesized polymer did not get enough time to crystallize and it reached to its melting point before finishing the crystallization process. Furthermore, the heat of fusion for polymerization also can be calculated as shown in Figure 4. 3.

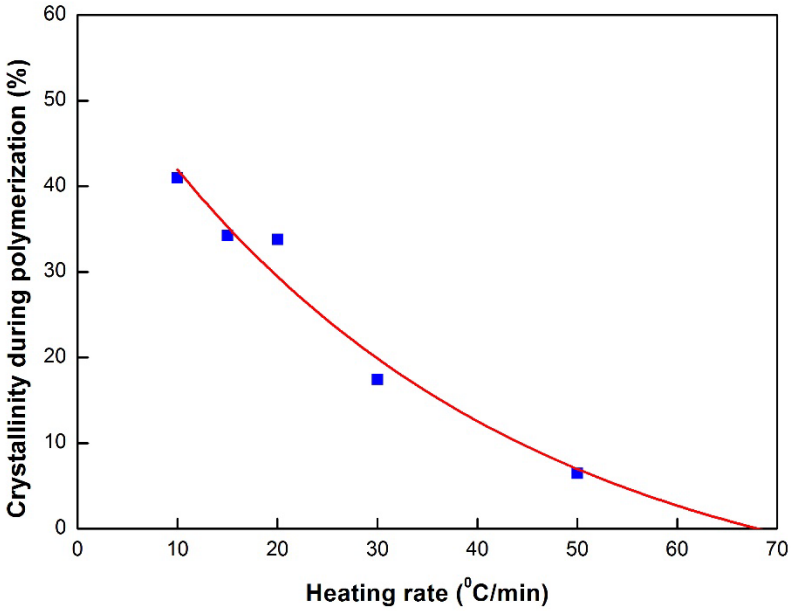

Figure 4. 2 Crystallinity at different heating rates during polymerization

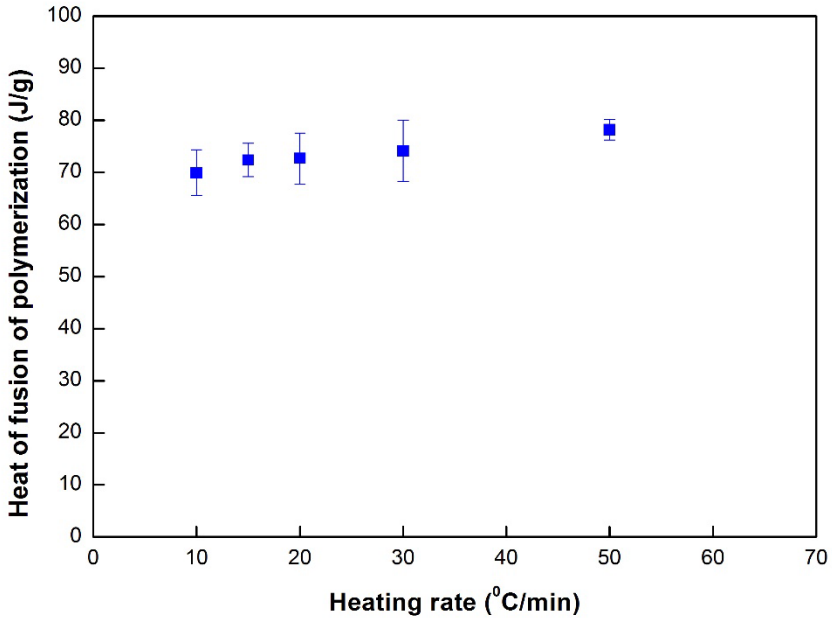

Figure 4. 3 Polymerization at different heating rates

4.1.2 Separation of polymerization and crystallization curves

Since polymerization and crystallization of ε-caprolactam occurs nearly simultaneously, so it is difficult to investigate polymerization and crystallization kinetics. Therefore, the exothermic peak in Figure 4. 1 can be separated by crystallization and polymerization peak (Figure 4. 4). Polymerization peak follows Gaussian distribution (Eq. (4.1)), whereas crystallization peak follows Maxwell-Boltzmann distribution (Eq. (4.2)).

$$f(x) = \frac{1}{\sigma\sqrt{2\pi}} e^{-\frac{(x-\mu)^2}{2\sigma^2}} \quad \textbf{(4.1)}$$

Where μ is mean or expectation of the distribution, σ is standard deviation and σ^2 is variance.

$$f(v) = f(v)\sqrt{(\frac{m}{2\pi kT})^3} \times \pi v^2 e^{-\frac{mv^2}{2kT}} \quad \textbf{(4.2)}$$

Where m is the particle mass, k is the product of Boltzmann's constant and T is thermodynamic temperature.

Eq. (4.1) and Eq. (4.2) can be simplified to Eq. (4.3) and Eq. (4.4) with the following parameters.

$$f(x) = A \times e^{B\times(x-C)^2} \quad \textbf{(4.3)}$$

$$f(v) = D \times v^2 \times e^{E\times v^2} \quad \textbf{(4.4)}$$

Figure 4. 4 represents the results from the separation of polymerization and crystallization using Gaussian distribution and Maxwell-Boltzmann distribution,

and the fitting data matches very well with the experimental facts at different heating rates.

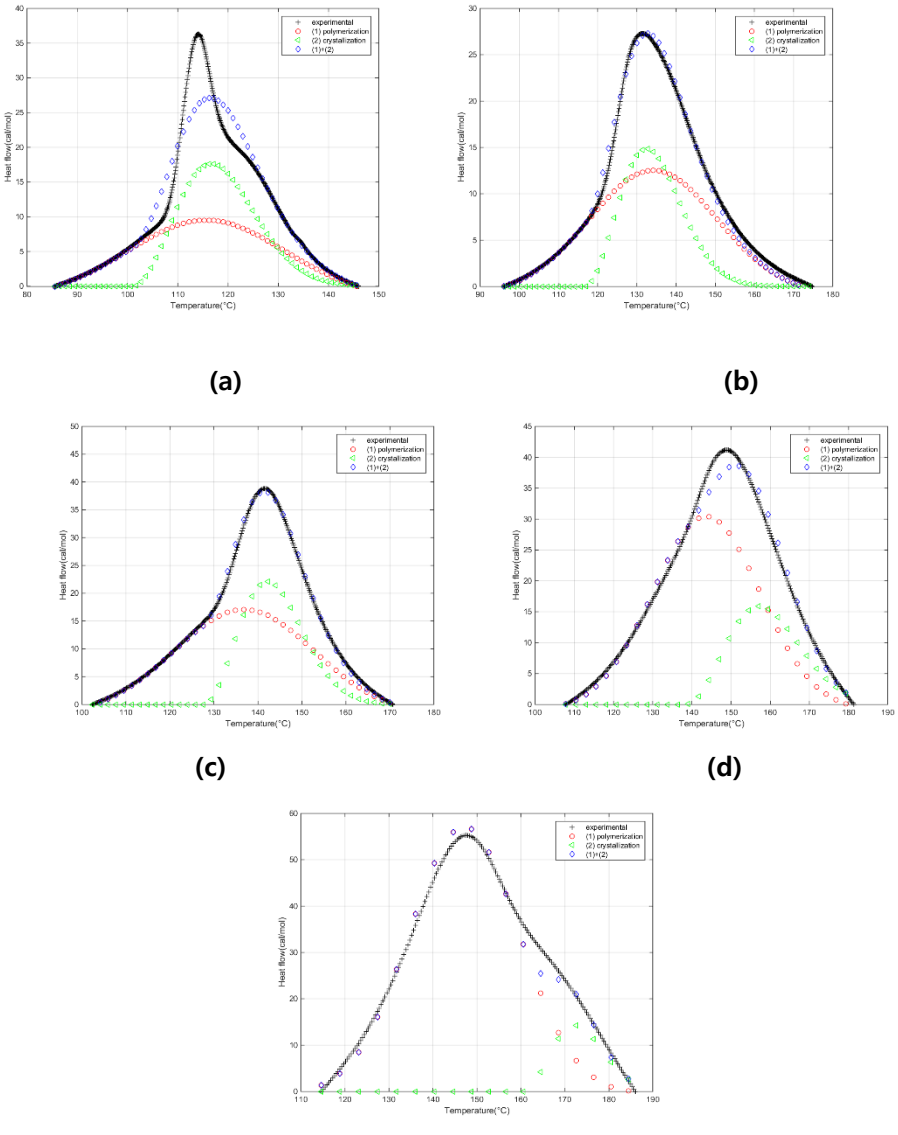

Figure 4. 4 Separation of polymerization and crystallization curve at different heating rates. (a) 10℃/min, (b)15℃/min, (c)20℃/min, (d)30℃/min, (e)50℃/min [40]

4.1.3 Modeling of polymerization kinetics at different heating rates

Researches on the kinetics of activated anionic polymerization of ε-caprolactam have been reported, and there are several autocatalytic reaction models for isothermal and non-isothermal polymerization [41].

The Arrhenius type autocatalytic model, which was proposed by Malkin et al. Eq. (4.5), describes the non-isothermal kinetics of caprolactam activated anionic polymerization in the bulk [42, 43].

$$\frac{d\alpha}{dt} = A_0 \exp(-\frac{E}{RT})(1-\alpha)^n\ (1 + B_0\alpha) \qquad \textbf{(4.5)}$$

Where A_0 is preexponential or frequency factor, E is activation energy, n is the order of reaction order, B_0 is autocatalytic factor, and α is the degree of conversion.

Besides that, a modification of Malkin's model has been suggested by Lin et al. They assume that the constant B_0 is not to be a constant, so Eq. (4.5) can be modified to the following Eq. (4.6). However, some disagreements have been existed, thus Lin's model has been almost completely abandoned in these days.

$$\frac{d\alpha}{dt} = A_0 \exp(-\frac{E}{RT})(1-\alpha)^n \ (1 + \frac{B_0'}{1-B_0'\alpha}\alpha) \qquad \textbf{(4.6)}$$

Furthermore, the autocatalytic model (Eq. (4.7)) has already been valid for many thermoset reactions [44, 45]. Recently, Teuwen et al. [46] reported that this model also can describe the activated anionic polymerization of caprolactam.

$$\frac{d\alpha}{dt} = \left[A_1 \exp\left(-\frac{E_1}{RT}\right) + A_2 \exp\left(-\frac{E_2}{RT}\right)\alpha^m\right](1-\alpha)^n \qquad \textbf{(4.7)}$$

Besides these models, there are many various modeling equations for polymerization kinetics. Among these models, Malkin's model (Eq. (4.5)) is the most frequently used model, and the first order autocatalytic reaction model (Eq. (4.8)) was used in this study for modeling of polymerization under non-isothermal condition. The reason why we use the first order autocatalytic reaction model is that we select the simplest formulas among the modeling equations which can fit the actual experimental data very well except chemical factors.

$$\frac{d\alpha}{dt} = A_0 \exp(-\frac{E}{RT})(1-\alpha) \ (1 + B_0\alpha) \qquad \textbf{(4.8)}$$

In Eq.s (4.8), there are three parameters A_0, E, B_0, and the commercial program Matlab was used for curve fitting and the parameters are summarized in Table 4. 2.

Figure 4. 5 represents that the relationship among polymerization rate (dα/dt), time (t), and the degree of conversion (α) at different heating rates. The results show that the fitting data matches very well with the experimental data, in other words, the first order autocatalytic reaction model is suitable for non-isothermal polymerization of ε-caprolactam.

Table 4. 2 Reaction parameters of the polymerization kinetics at different heating rates

Heating rate (℃/min)	A_0	E	B_0
10	0.0583	3000	6.005
15	0.0675	3380	6.054
20	0.116	3680	6.382
30	0.2741	4370	6.488
50	0.7093	4920	6.498

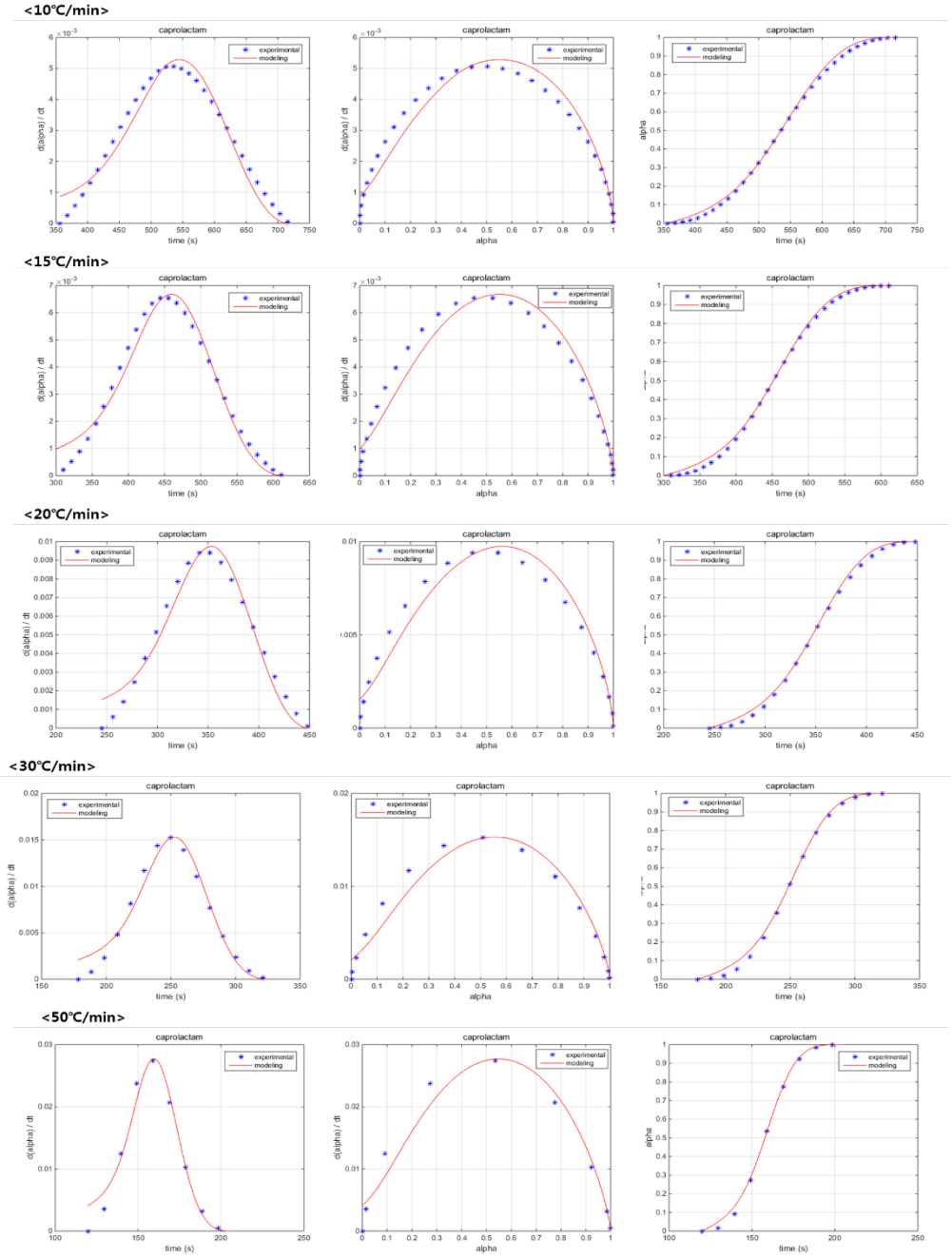

Figure 4. 5 Comparison of modeling results with experimental data using the 1st order autocatalytic reaction model

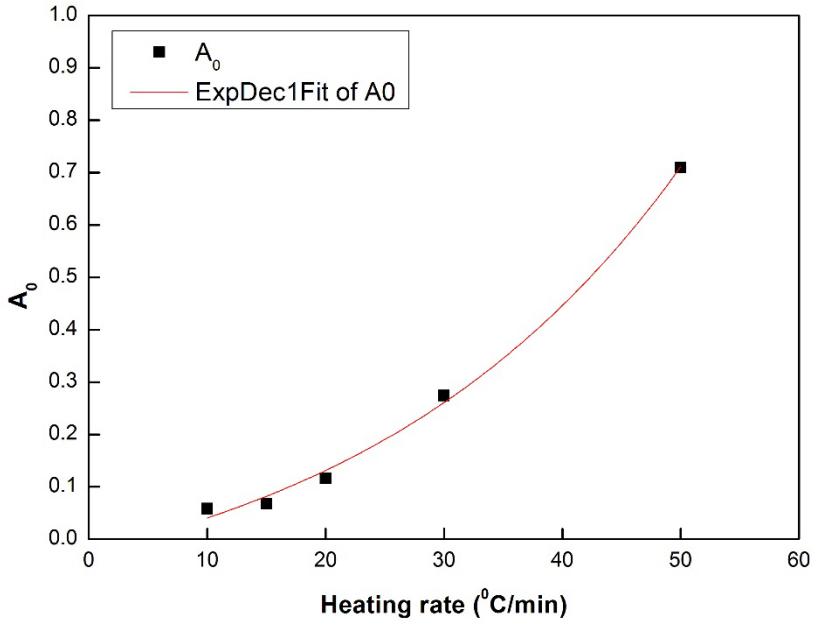
A0
ExpDec1Fit of A0
A0
Heating rate (0C/min)

(a)

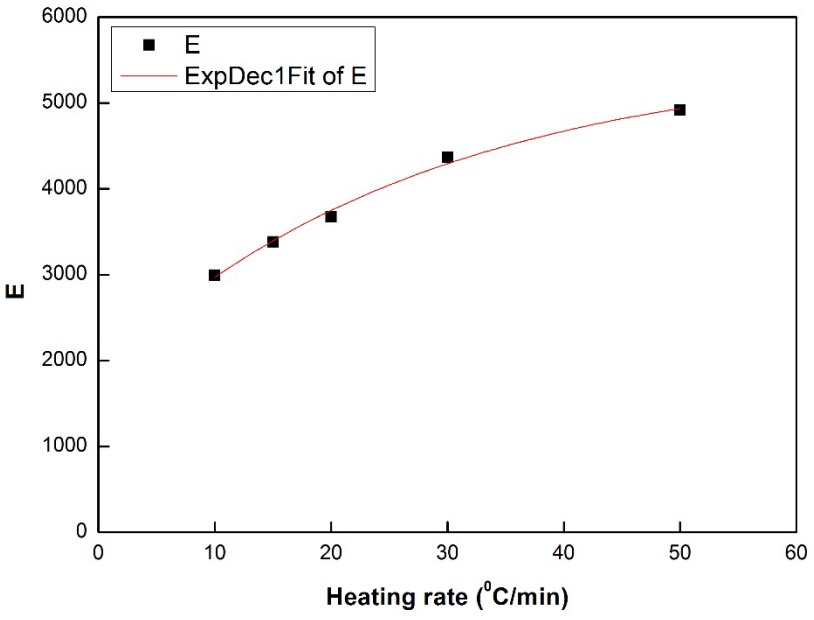
E
ExpDec1Fit of E
E
Heating rate (0C/min)

(b)

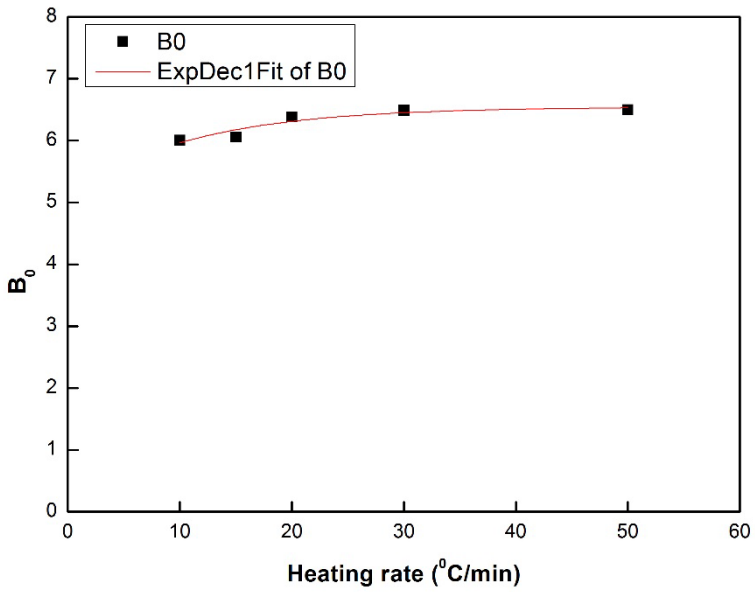

(c)

Figure 4. 6 Kinetic parameters for polymerization of ε-caprolactam at different heating rate.

Table 4. 3 Reaction parameters of the polymerization kinetics at different heating rate using exponential curves in Figure 4. 6

Heating rate (℃/min)	A_0	E	B_0
10	0.0407	2970	5.963
15	0.0819	3390	6.175
20	0.1312	3750	6.310
30	0.2607	4290	6.450
50	0.7108	4940	6.530

According to the exponential curves in Figure 4. 6, we can obtain three kinetic parameters at a specified heating rate (Table 4. 3), and also predict the polymerization kinetics at this heating rate (Figure 4. 7).

Figure 4. 7 shows that the modeling results follows the experimental data, namely the first order autocatalytic reaction model is suitable for describing a non-isothermal polymerization.

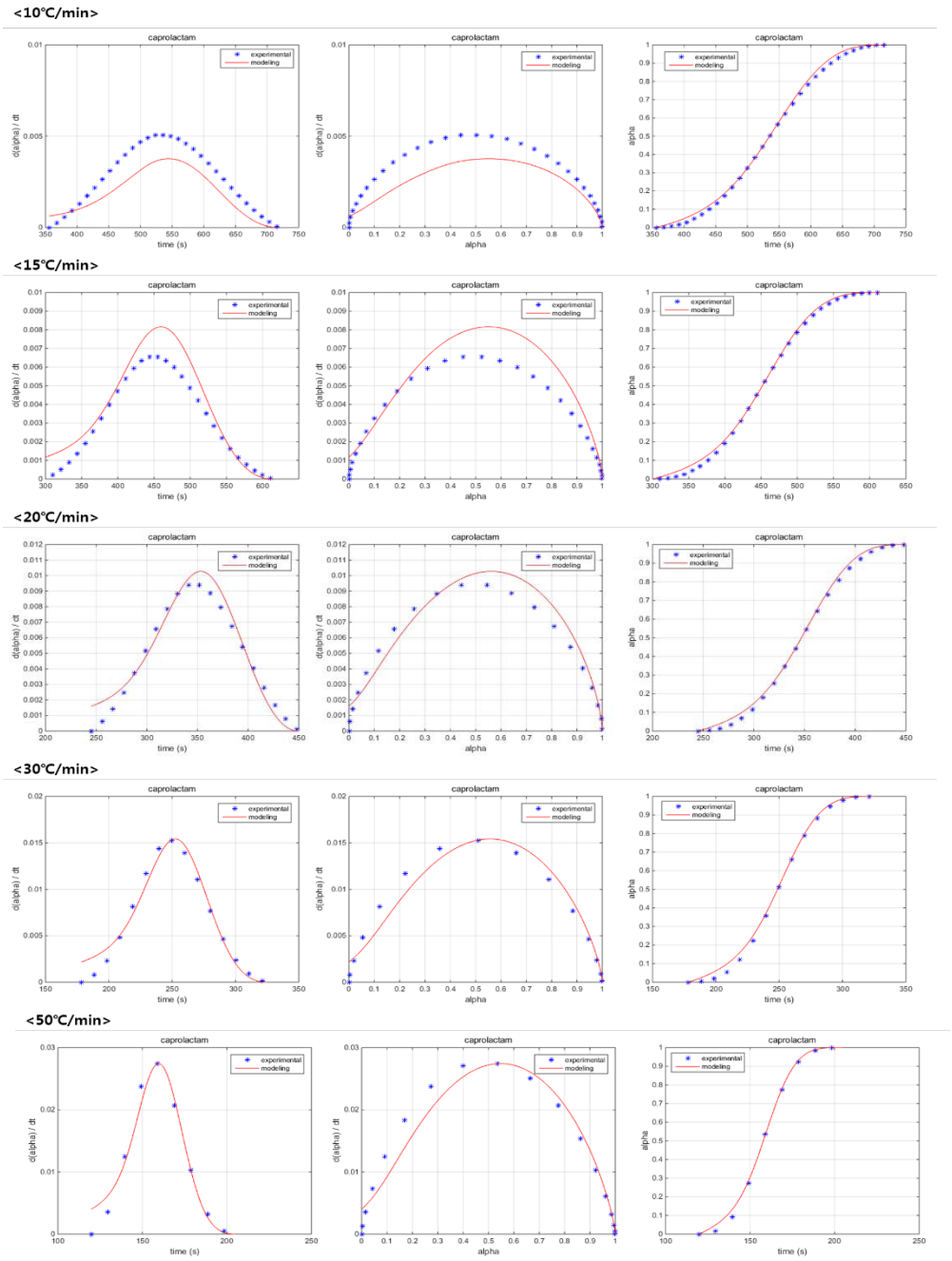

Figure 4. 7 Comparison of modeling results with experimental data using exponential fitting parameters

4.2 Isothermal scanning

In order to investigate the polymerization and crystallization kinetics of ε-caprolactam at different molding temperatures, isothermal scanning was done.

4.2.1 Scanning process

First, DSC samples were heated at a specified molding temperature for 5 minutes and then cooled down to room temperature. After that, they were heated from room temperature to 250℃ at the heating rate of 10℃/min to evaluate the degree of polymerization and crystallinity during isothermal scanning process. Finally, these samples were cooled in the liquid nitrogen and then heated from room temperature to 250℃ at the heating rate of 10℃/min.

4.2.2 Analysis of polymerization kinetics during isothermal scanning

At lower temperature, crystallization and polymerization occurs at the same time, because at lower reaction temperature monomer could be trapped inside of the crystals before being able to polymerize. However, at high temperature, the growth of the chains is more significant than the formation of crystals (Figure 4.

8). It means that the molding temperature adversely affect both polymerization rate and crystallization rate; therefore, there is an optimum molding temperature for good properties of polymers.

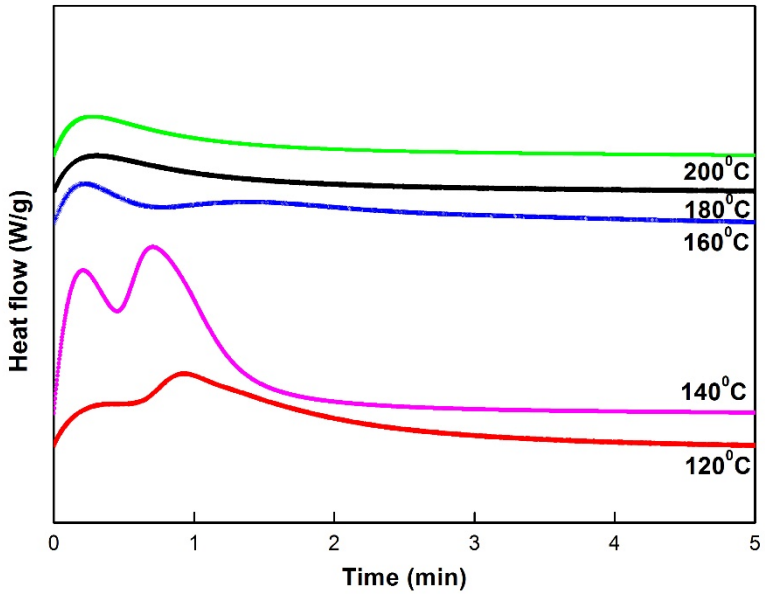

Figure 4. 8 DSC thermograms of isothermal scanning process

As shown in Table 4. 4, the heat of reaction for isothermal scanning process increases at lower temperature (120℃-140℃) and then decreases as increasing of molding temperature.

During isothermal process, we also can obtain the degree of polymerization data over time, which is essential for the following chapter to perform simulation analysis.

Table 4. 4 DSC diagrams of isothermal scanning process

Molding temperature (℃)	120℃	140℃	160℃	180℃	200℃
Heat of reaction (J/g)	94.48	144.00	94.29	37.80	36.18

Figure 4. 9 demonstrates that there exists much unreacted monomer after isothermal for 5 minutes at 120℃, whereas no endothermic peak appears at other temperatures, in other words, most monomer was converted to PA6 at several molding temperatures except 120℃. Furthermore, at low molding temperature (140℃-160℃), little exothermic peak presents at around 70℃ due to fully crystallization during isothermal process. However, samples, which were isothermal heated at high temperature (180℃-200℃), were recrystallized during the first heating process because polymerization rate is higher than crystallization rate at high temperature; therefore, few crystals can be formed at high temperature.

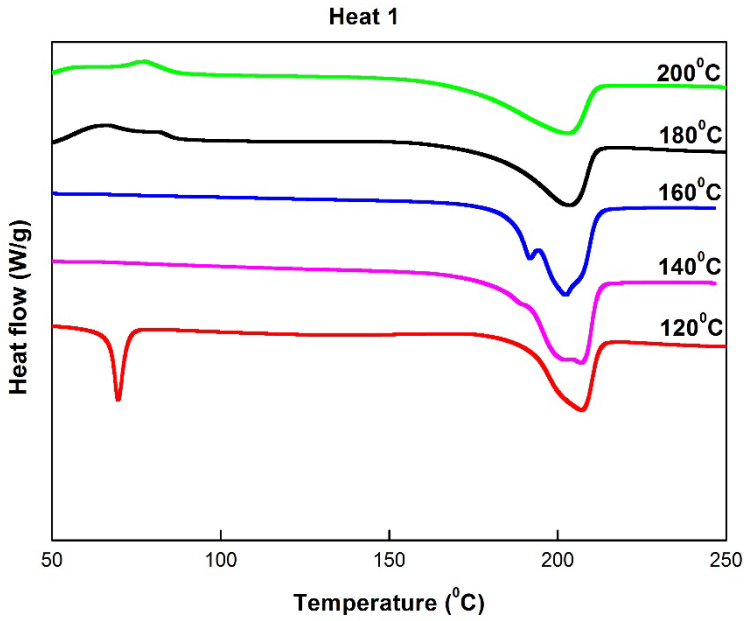

Figure 4. 9 DSC diagrams of the first heating process

Table 4. 5 DSC diagrams of the first heating process

Molding temperature (℃)	First heating		
	Endothermic reaction (J/g)	Melting (J/g)	T_m (℃)
120℃	-16.36	51.57	206.86
140℃	1.12	81.69	206.72
160℃	0.43	76.33	202.40
180℃	24.92	61.54	203.08
200℃	23.02	62.23	202.31

In addition, the polymer melting temperature slightly decreased with an increase of molding temperature (Table 4. 5). It means that crystals formed during isothermal scanning process leads to higher melting temperature.

The first heated samples were cooled in liquid nitrogen in order to prevent recrystallization during the cooling process and these were reheated from room temperature to 250℃ to investigate whether there still exist unreacted monomer and the crystallization behavior. Consequently, all the samples were fully polymerized after isothermal heating and dynamic heating process. Those were crystallized at around 74℃ and heat of reaction for crystallization is about 25 J/g (Figure 4. 10 & Table 4. 6).

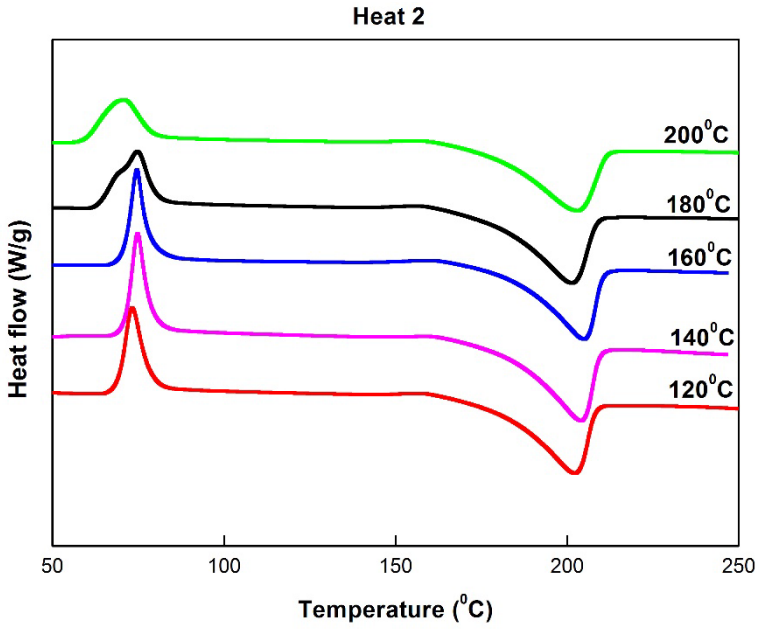

Figure 4. 10 DSC diagrams of the second heating process

Table 4. 6 DSC diagrams of the second heating process

Molding temperature (℃)	Second heating			
	Crystallization (J/g)	T_c (℃)	Melting (J/g)	T_m (℃)
120℃	25.60	73.27	66.51	201.90
140℃	26.66	74.82	65.55	203.94
160℃	25.55	74.60	62.96	204.61
180℃	27.36	74.76	67.95	201.05
200℃	24.51	74.77	69.38	201.43

CHAPTER 5. Numerical Analysis

Since ε-caprolactam is polymerized in a short time, the overall process must be done within a critical processing time, which is an important parameter in molding parts of various sizes and shapes. In addition, viscosity of polymerizing ε-caprolactam also changes rapidly depending on polymerization time.

In this chapter, a critical processing time will be defined, and numerical simulation was performed to evaluate the relationship between filling ratio and filling time. The commercial software “Fluent” was used using a user defined function.

5.1 Governing equations and methods

The following governing equations are used under the assumption that the viscous fluids is incompressible. The incompressible flow refers to a flow in which the changes of the fluid density can be negligibly small compared to the base density.

Mass conservation equation:

$$\nabla \cdot \mathbf{u} = 0 \tag{5.1}$$

$$\frac{\partial_{u_i}}{\partial_{x_i}} = 0$$

Momentum conservation equation:

$$\rho\left(\frac{\partial_{\boldsymbol{u}}}{\partial_t} + \mathbf{u} \cdot \nabla \mathbf{u}\right) = \nabla \cdot \boldsymbol{\sigma} + \rho \mathbf{S} \tag{5.2}$$

$$\rho\left(\frac{\partial_{u_i}}{\partial_t} + u_i u_{i,j}\right) = \nabla \cdot \sigma_{ij} + \rho S_i$$

Constitutive equation:

$$\boldsymbol{\sigma} = \boldsymbol{\tau} - \mathrm{p}\mathbf{I}\ ;\ \boldsymbol{\tau} = 2\mu_f \boldsymbol{D} \tag{5.3a}$$

$$\mathbf{D} = \frac{1}{2}[(\boldsymbol{\nabla u}) + (\boldsymbol{\nabla u})^{\boldsymbol{T}}]$$

$$\sigma_{ij} = \tau_{ij} - p\delta_{ij}\ ;\ \tau_{ij} = 2\mu_f D_{ij} \tag{5.3b}$$

$$D_{ij} = \frac{1}{2}\left(\frac{\partial u_i}{\partial x_j} + \frac{\partial u_j}{\partial x_i}\right)$$

Where **u**, ρ, **σ**, **S**, **τ**, p and **D** are the velocity vector, the density, the total stress tensor, the body forces, the viscous stress tensor, the pressure and the strain rate tensor, respectively.

The flow front was defined by the VOF method, which was first developed by Hirt and Nichols [47]. It is the representative algorithm based on a fixed coordinate system for solving flows with moving free surfaces. The volume fluid *f* is defined as the volume fraction of a fluid in an element, which can be expressed as

$$f = \frac{\text{volume of fluid}}{\text{volume of element}}$$

If an element is completely charged with the fluid, the volume of fluid is unity ($f = 1$). Meanwhile, an element is empty ($f = 0$), it belongs to the empty region and its contribution to the calculation of flow field is excluded. If elements are partially charged, the elements are considered to be on the free surface and the volume of fluid is between 0 and 1 ($0 < f < 1$). In this study, the location of the flow is defined as a point where the fluid fraction has a value of 0.5 ($f = 0.5$). As shown in Figure 5. 1, the calculation field with free surface can be easily represented by using the variable *f*.

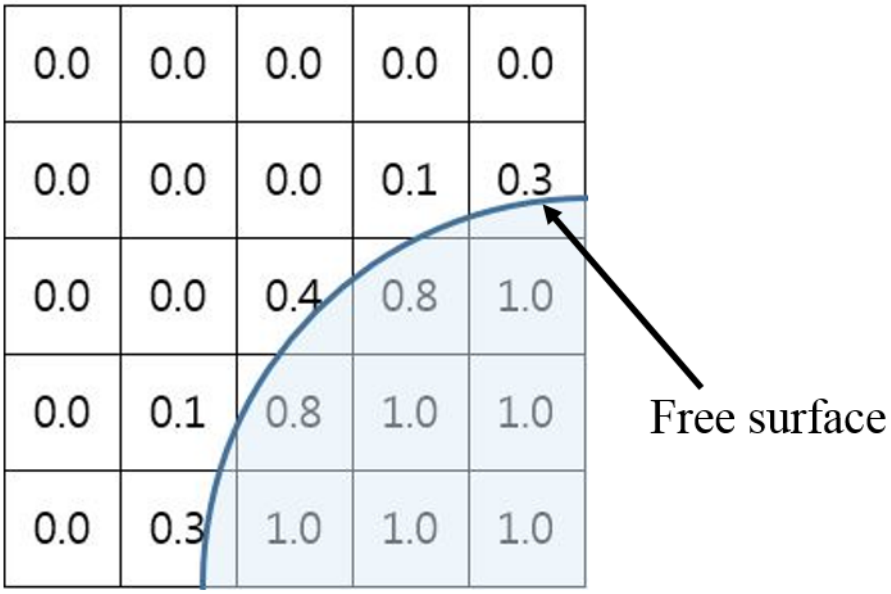

Figure 5. 1 Schematics of volume of fluid (VOF) method

Generally, the fiber reinforcements in the mold for resin transfer molding can be regarded as porous media. When the resin is injected into the mold, the resin flows through small gaps between the fibers. The most generally accepted equation to describe the porous media is Darcy's law (Eq.s (5.4)), which was formulated by Henry Darcy based on the results of experiments on the flow of water through beds of sands, forming the basis of hydrogeology, a branch of earth science [48].

Figure 5. 2 shows the flow in the simply form of porous media.

Figure 5. 2 Illustration for porous media flow

$$v = -\frac{K}{\mu}\frac{dP}{dx} \tag{5.4}$$

Where v is velocity of the flow, K is permeability of the medium, μ is viscosity of the polymerizing ε-caprolactam which depends on time and temperature, P is pressure and x is the distance of flow front (Figure 5. 2).

In Eq.s (5.4), velocity of the flow also can be described as Eq.s (5.5), and the relationship between viscosity and the distance of flow front (Eq.s (5.6)) can be obtained through the following integration steps.

$$v = \frac{dx}{dt} \tag{5.5}$$

$$\therefore \frac{dx}{dt} = -\frac{K}{\mu}\frac{dP}{dx}$$

$$\int x\,dx = \int \frac{KP}{\mu}\,dt$$

$$\frac{1}{KP}\int x\,dx = \int \frac{1}{\mu}\,dt$$

$$\int_0^{t_{gel}} \frac{1}{\mu}\,dt = \frac{x^2}{2KP}$$

$$\int_0^{t_{gel}} \frac{1}{\mu}\,dt \propto x^2 \qquad \textbf{(5.6)}$$

From Eq.s (5.6), we can calculate the relative relationship between viscosity and the distance of the flow front. Because the viscosity of polymerizing ε-caprolactam varies with temperature and time (Figure 5. 3), time dependent viscosity of ε-caprolactam monomer at a specified temperature can be required.

However, the ε-caprolactam monomer can be polymerized rapidly, thus the molding process must be finished in a short time. Therefore, the viscosity data for the first 30 seconds is required in order to analyze the flow in the mold. However, the initial viscosity of the ε-caprolactam monomer is 3 to 4 times that

of water and polymerization reaction rate is fast, moreover, the equipment that can measure low viscosity has a limitation to temperature, thus it is challenge to measure the viscosity change within the first 30 seconds.

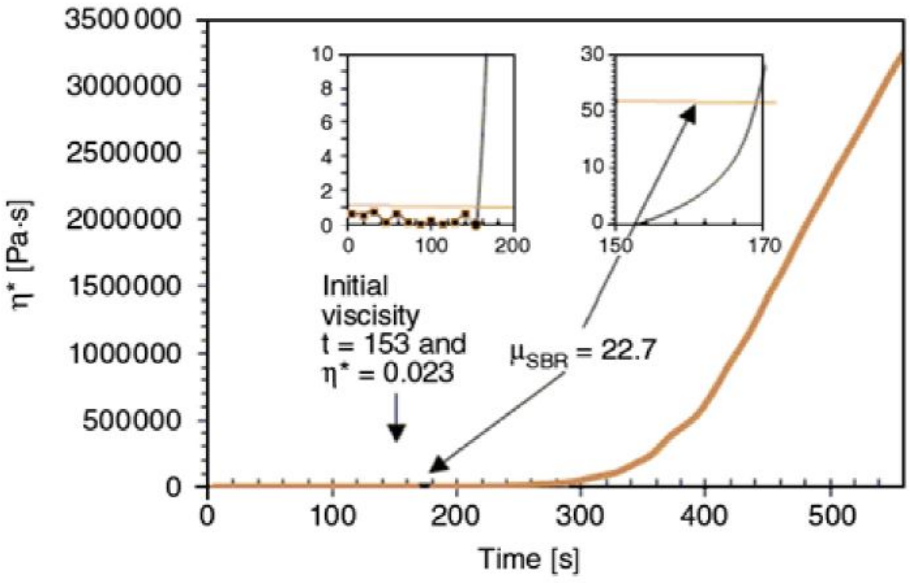

Figure 5. 3 Viscosity-time profile of CL/C1/C20 (100/4/4) at 150℃ [49]

Dave et al. [50] reported that below 50% conversion for polymerization, the complex relative viscosity ($|\eta^*|/|\eta_0^*|$) values were linear in relation to conversion for polymerization, and the viscosity of ε-caprolactam monomer can be described by the following (Eq.s (5.7) & Eq.s (5.8)). The change in viscosity

of the monomer during polymerization is assumed to be exponentially dependent on the polymer conversion X, which is attributed to the formation and the growth of the polymer chains.

$$|\eta^*| = |\eta_0^*| \exp(kX) \qquad (X < 0.5) \tag{5.7}$$

Where $|\eta^*|$ is the complex viscosity of PA6 anionically polymerizing in its monomer, $|\eta_0^*|$ is the complex viscosity of caprolactam monomer, k is a constant, and X is fractional conversion. The complex viscosity of the monomer, $|\eta_0^*|$, follows an Arrhenius temperature dependence

$$|\eta_0^*|(\mathrm{T}) = 2.7 \times 10^{-7} \exp(3525/T) \text{ (Pa.s)} \tag{5.8}$$

Figure 5. 4 shows time dependent viscosity of polymerizing ε-caprolactam at specified temperatures. At early stage, viscosity varies almost linearly with the time; however, that at 200℃ rapidly increases from 20 seconds. Moreover, the viscosity at 120℃ increases slowly which means polymerization rate is slower than that of other cases (Figure 5. 5).

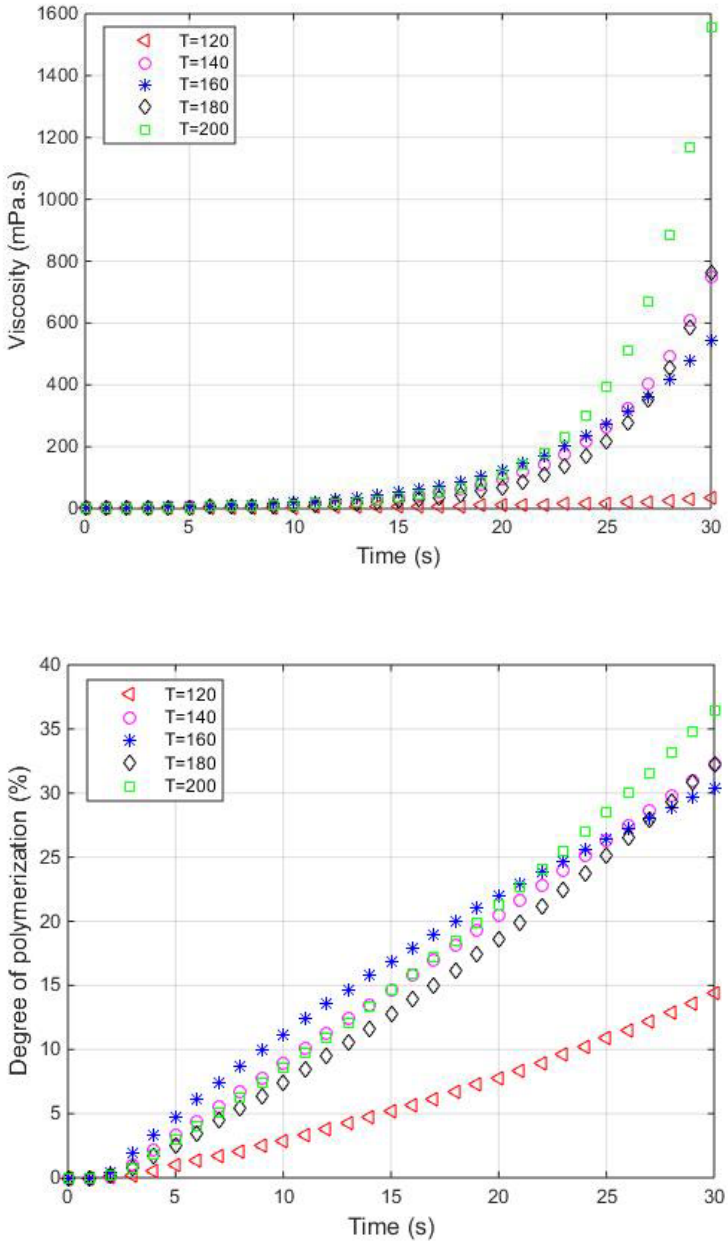

Figure 5. 4 Viscosity-time profile of ε-caprolactam during the first 30 seconds at different temperatures

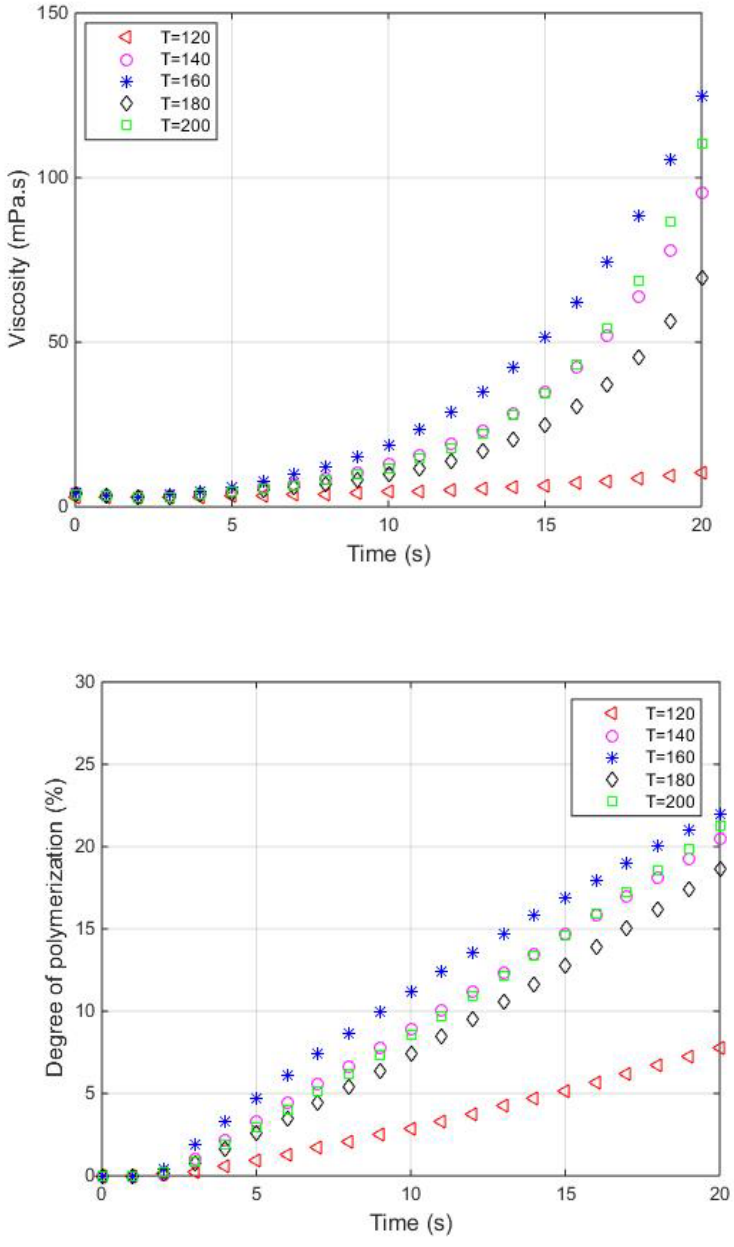

Figure 5. 5 Viscosity-time profile of ε-caprolactam during the first 20 seconds at different temperatures

As mentioned above (Figure 5. 4 and Figure 5. 5), viscosity of polymerizing ε-caprolactam varies with filling time, from these data we can obtain the relationship between filling time and the parameter which related to viscosity or the distance of flow front (Figure 5. 6). A time when the distance of flow front has no change can be defined as the critical processing time (Figure 5. 7), and the molding process must be finished within the critical processing time (20 seconds), regardless of the shape and size of the parts.

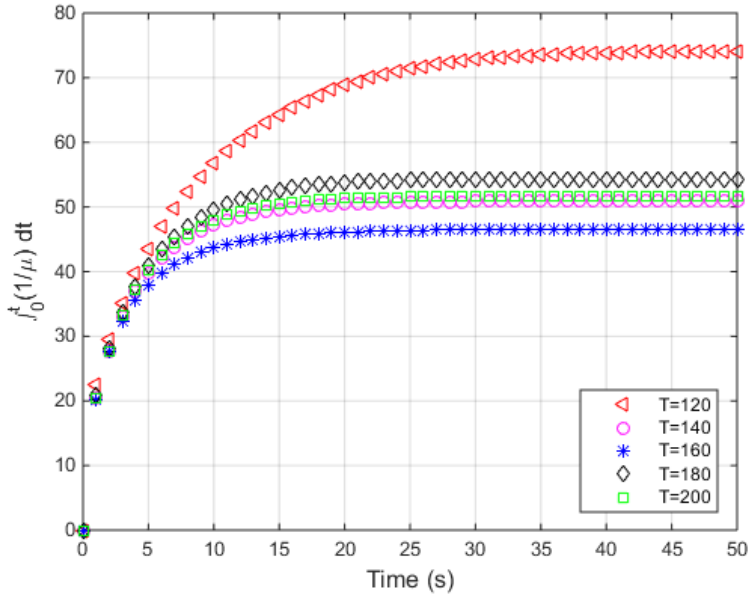

Figure 5. 6 Relationship between filling time and parameter of viscosity

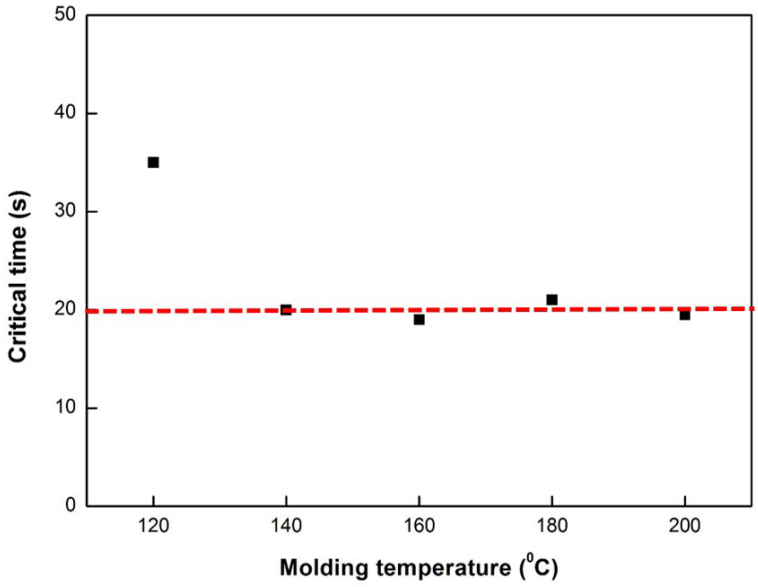

Figure 5. 7 Critical time at different molding temperatures

5.2 Simulation results

5.2.1 Flow in a rectangular mold

The mold geometry is shown in Figure 5. 8, and the size of porous zone is 180mm by 180mm. The resin flows along the runner first, and then flows into porous zone. There are two inlets in non-porous zone and one outlet in porous zone.

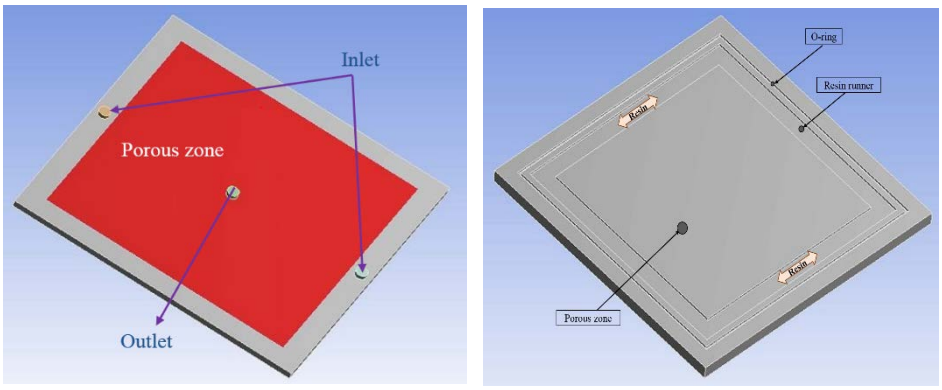

Figure 5. 8 Geometry of rectangular mold

As the resin flows along the runner first and then flows into the porous zone, the geometry of mold can be simplified as the porous zone with four inlets and one outlet in the middle (Figure 5. 9). The resin is injected at a constant pressure to the mold; thus pressure boundary condition was used for the inlet boundary conditions. Numerical analysis was performed with respect to five cases of 120℃, 140℃, 160℃, 180℃ and 200℃, which have different viscosity tendencies that varied with processing time. The gauge pressure of inlet is 0.85 bar and outlet pressure is atmospheric pressure for all cases.

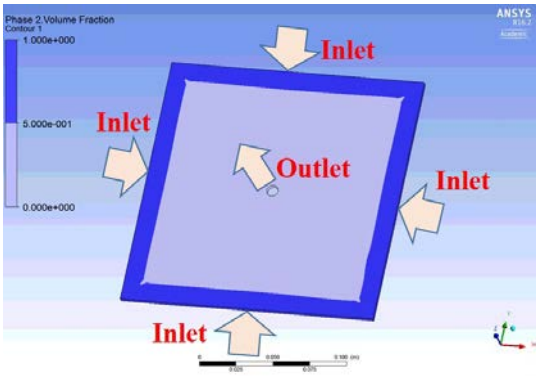

Figure 5. 9 Simplified mold

The time dependent viscosity of polymerizing ε-caprolactam is set using user defined function (UDF), and the permeability of woven carbon fabric is $K_1=K_2=8.0 \times 10^{-11} m^2$, $K_3=4.0 \times 10^{-12} m^2$ [51].

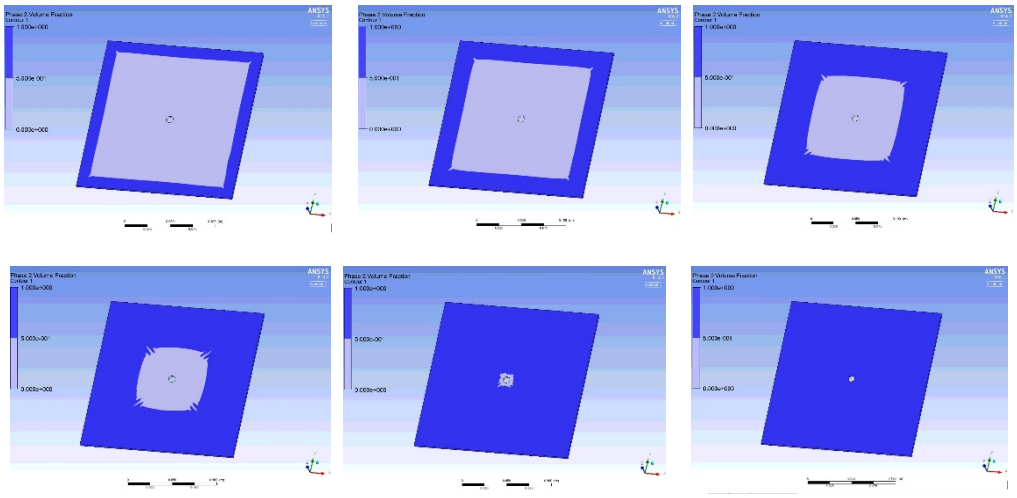

Figure 5. 10 Phase contours in carbon fabric with various molding temperatures

The phase contour results are shown in Figure 5. 10. The results show that the mold is fully filled with resin within 5 seconds which is shorter than critical processing time (Figure 5. 11). Comparing the experimental results with the simulation results, the injection times of all cases are within 5 seconds.

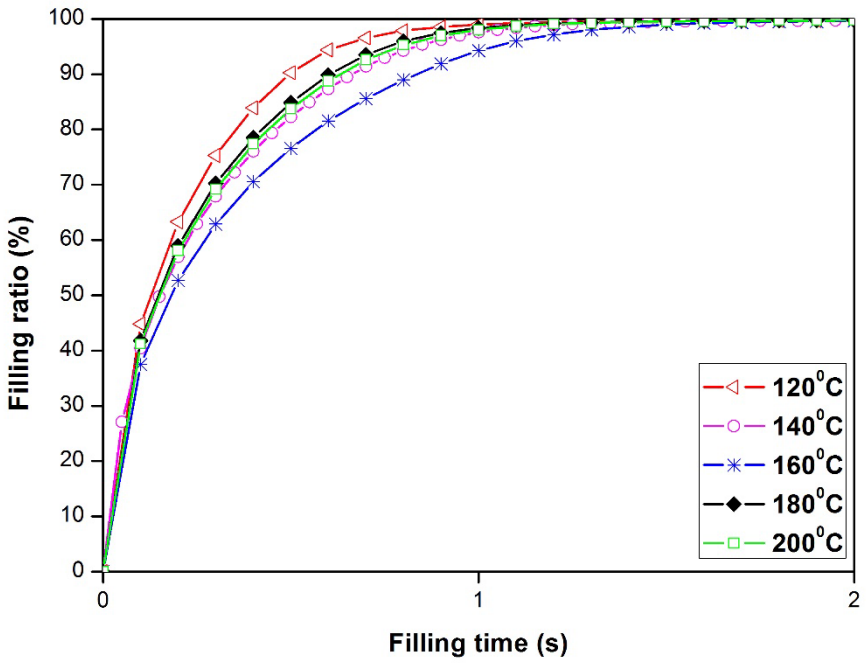

Figure 5. 11 Relationship between filling time and filling ratio at different molding temperatures

5.2.2 Flow in an automotive part with one or three inlets

In order to evaluate the processing time for the real size hood of an automobile, simulation was conducted. The time dependent viscosity of polymerizing ε-caprolactam at 140℃ is set using user defined function (UDF) for this numerical analysis, and the permeability of woven carbon fabric is the same as mentioned above. The size of hood is 1200mm by 1700mm, and the simulation was divided into two conditions (Figure 5. 12 and Figure 5. 13).

The resin is injected at a constant pressure to the mold; thus pressure boundary condition was used for the inlet boundary conditions, too. Numerical analysis was performed with respect to five or six cases of pressure with the same viscosity data.

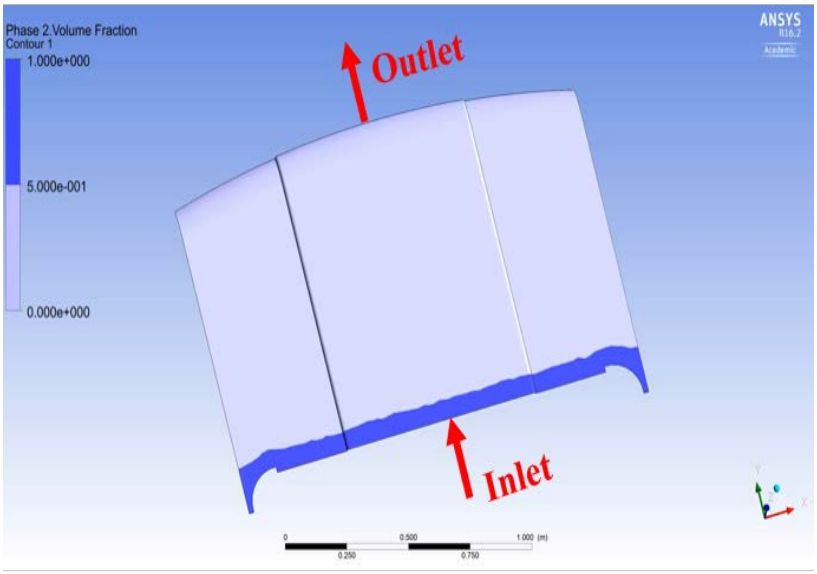

Figure 5. 12 Geometry of automotive part with one inlet

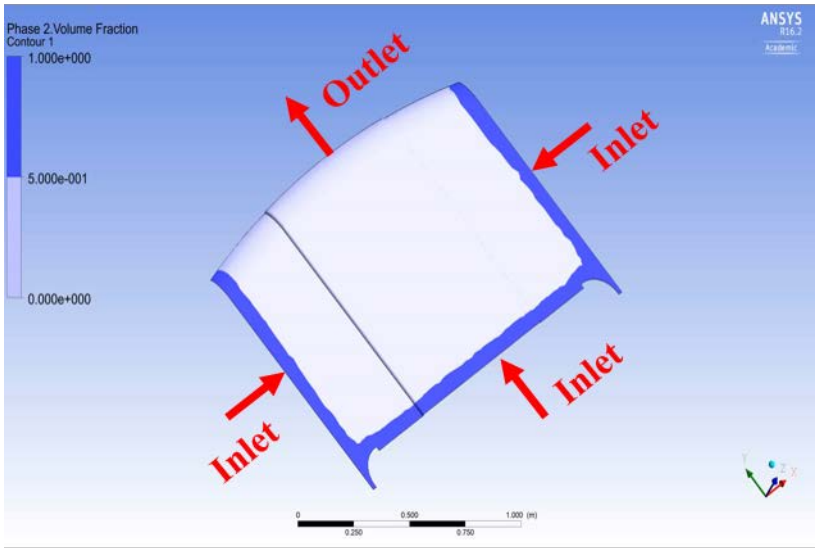

Figure 5. 13 Geometry of automotive part with three inlets

Phase contour in carbon woven fabric for automotive hood with one inlet is shown in case of 10 bar to 60 bar inlet pressure in Figure 5. 14 to Figure 5. 19, and the filling ratio at the critical processing time in each case is summarized in Table 5. 1. The results show that if only one inlet and one outlet are used, the resin injection can be completely finished within the critical processing time at a pressure of 60 bar.

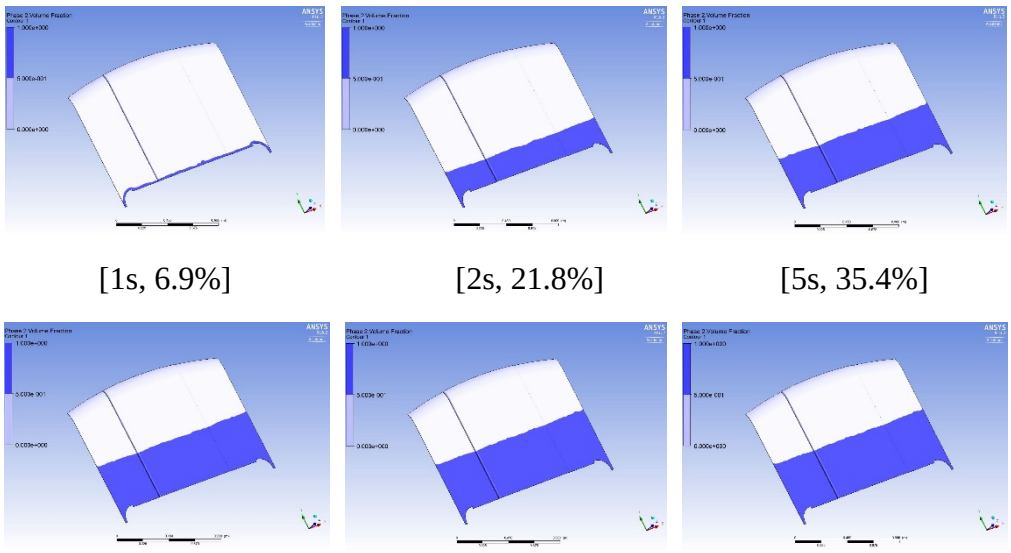

[1s, 6.9%] [2s, 21.8%] [5s, 35.4%]

[10s, 42.0%] [20s, 44.9%] [25s, 45.2%]

Figure 5. 14 Phase contours in CFRTP composites with one inlet at 10 bar

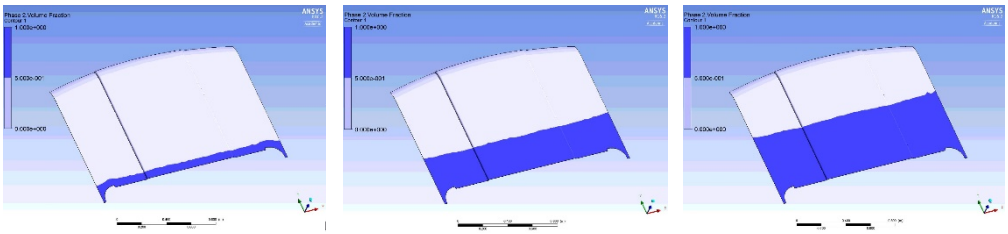

[1s, 6.9%] [2s, 30.2%] [5s, 49.4%]

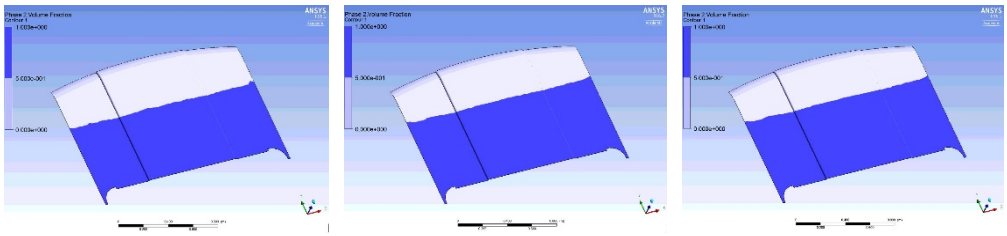

[10s, 58.7%] [20s, 62.9%] [25s, 63.3%]

Figure 5. 15 Phase contours in CFRTP composites with one inlet at 20 bar

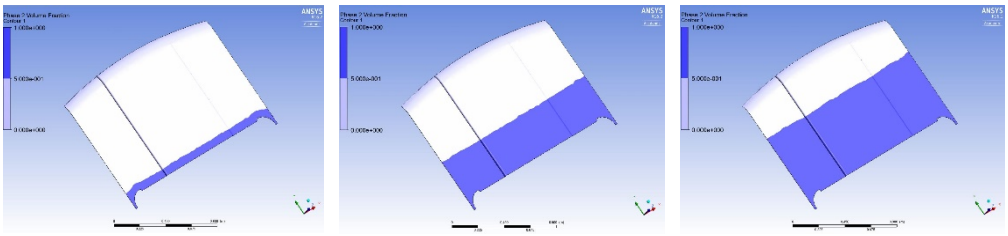

[1s, 6.9%] [2s, 36.7%] [5s, 60.1%]

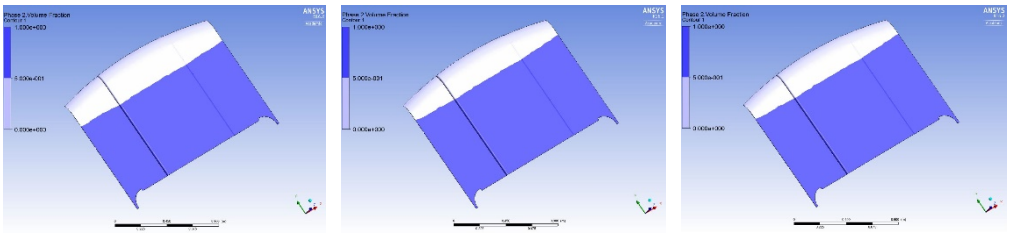

[10s, 71.4%] [20s, 76.6%] [25s, 77.1%]

Figure 5. 16 Phase contours in CFRTP composites with one inlet at 30 bar

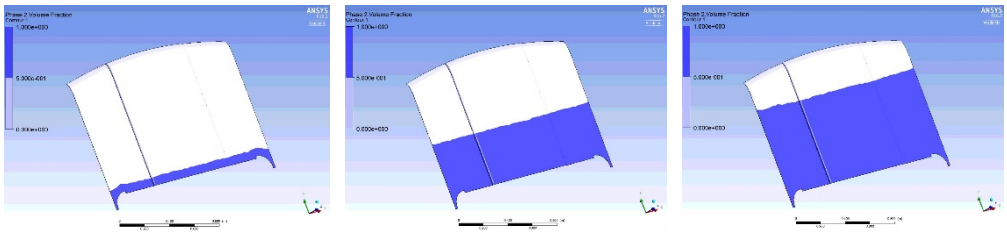

[1s, 6.9%] [2s, 42.2%] [5s, 69.1%]

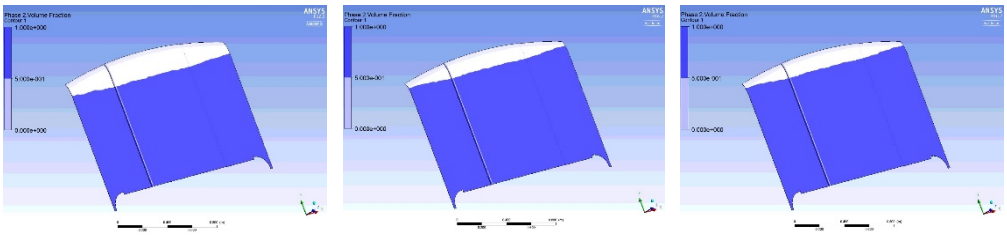

[10s, 82.2%] [20s, 88.2%] [25s, 88.7%]

Figure 5. 17 Phase contours in CFRTP composites with one inlet at 40 bar

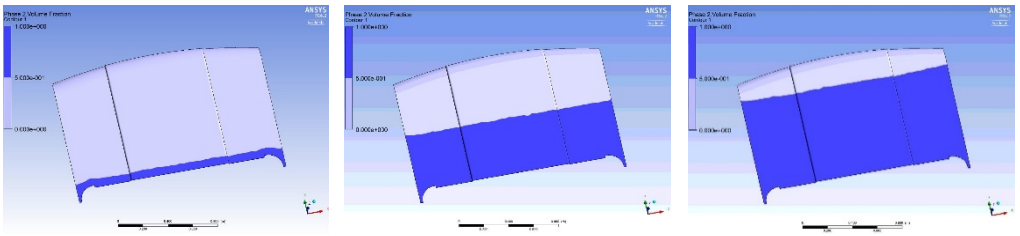

[1s, 6.9%] [2s, 47.1%] [5s, 77.0%]

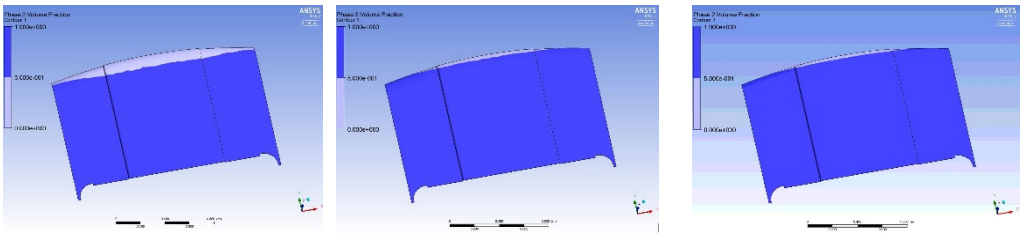

[10s, 91.6%] [20s, 97.7%] [25s, 98.1%]

Figure 5. 18 Phase contours in CFRTP composites with one inlet at 50 bar

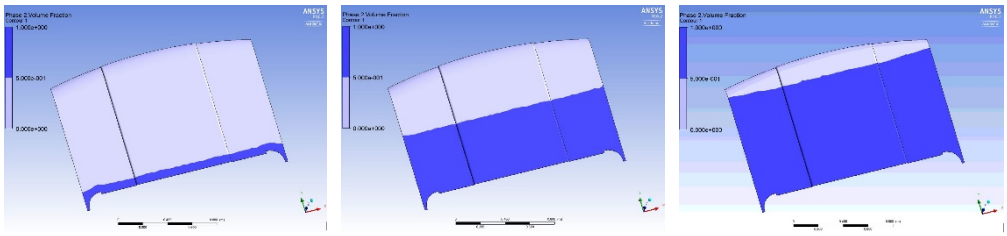

[1s, 6.9%] [2s, 51.6%] [5s, 84.2%]

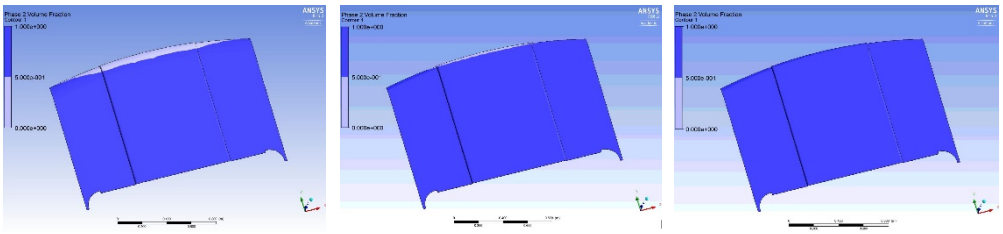

[8s, 95.6%] [10s, 98.8%] [15s, 100%]

Figure 5. 19 Phase contours in CFRTP composites with one inlet at 60 bar

Table 5. 1 Filling time and filling ratio at different pressures with one inlet

Molding temperature (℃)	Inlet pressure (bar)	Filling time (s)	Filling ratio (%)
140℃	10	20	44.9
	20	20	62.9
	30	20	76.6
	40	20	88.2
	50	20	97.7
	60	15	100

Simulations were performed with three inlets and one outlet in order to finish the molding within the critical processing time with lower pressure.

Phase contour in carbon woven fabric for automotive hood with three inlets is shown in case of 10 bar to 50 bar inlet pressure in Figure 5. 20 to Figure 5. 24, and the filling ratio at the critical processing time in each case is summarized in Table 5. 2. The results show that if three inlets and one outlet are used, the resin injection can be completely finished within the critical processing time at a pressure of 40 bar, which is only two-thirds of the value with one inlet case.

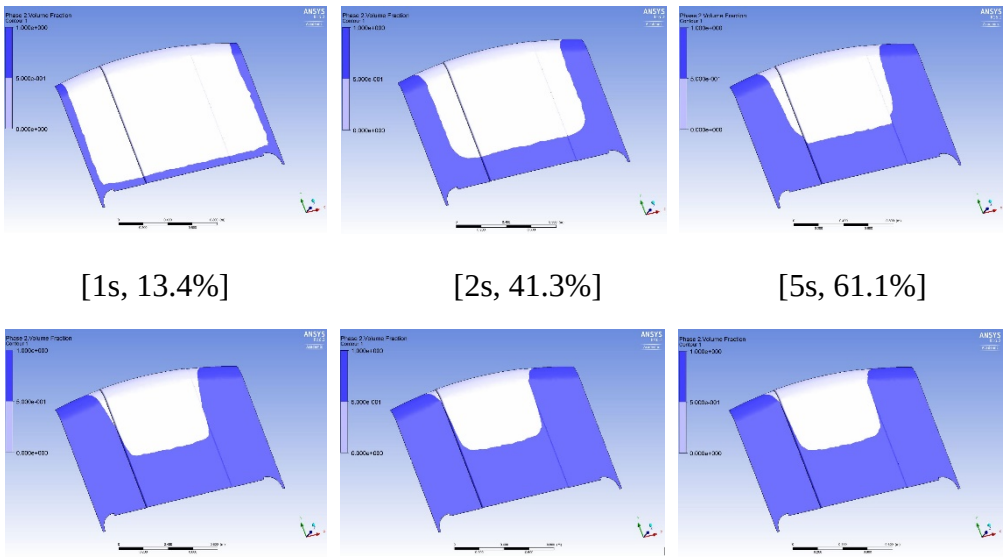

[1s, 13.4%] [2s, 41.3%] [5s, 61.1%]

[10s, 69.6%] [20s, 72.7%] [25s, 73.0%]

Figure 5. 20 Phase contours in CFRTP composites with three inlets at 10 bar

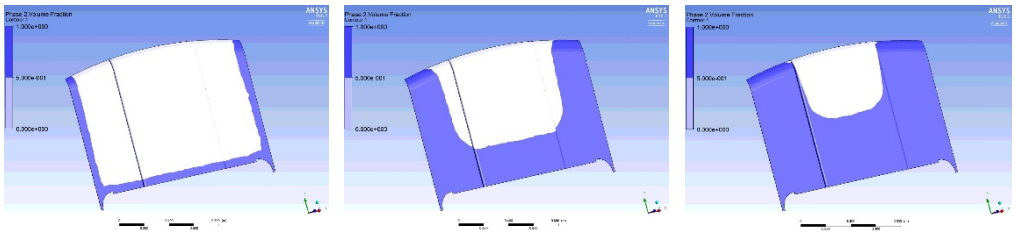

[1s, 13.4%] [2s, 54.6%] [5s, 77.2%]

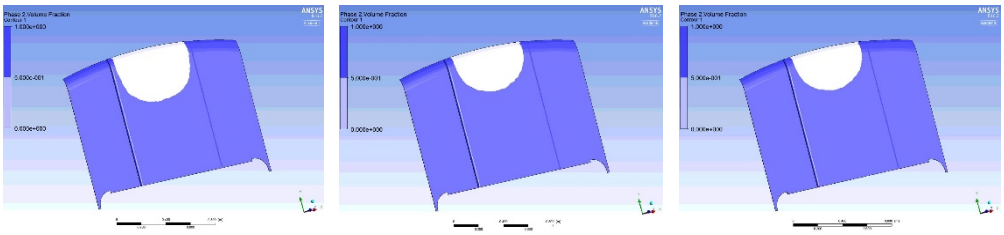

[10s, 84.3%] [20s, 88.5%] [25s, 88.9%]

Figure 5. 21 Phase contours in CFRTP composites with three inlets at 20 bar

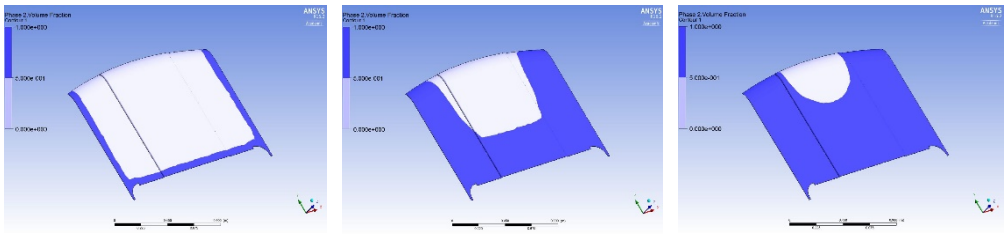

[1s, 13.4%] [2s, 63.7%] [5s, 85.5%]

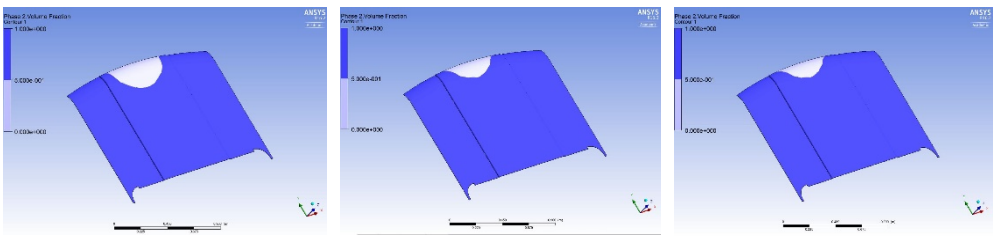

[10s, 93.0%] [20s, 96.0%] [25s, 96.2%]

Figure 5. 22 Phase contours in CFRTP composites with three inlets at 30 bar

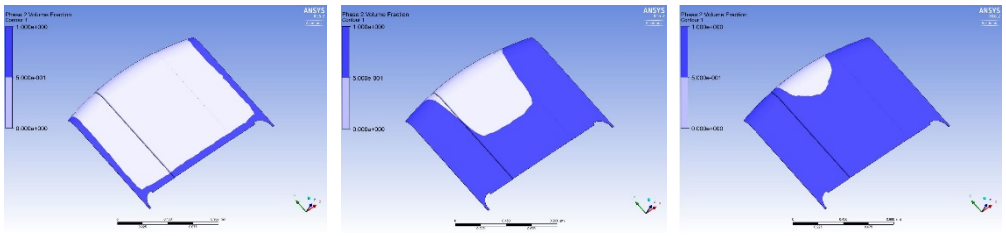

[1s, 13.4%] [2s, 70.8%] [5s, 92.0%]

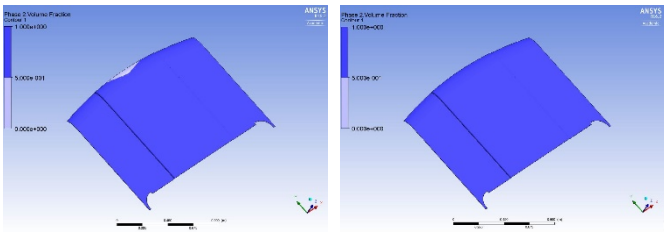

[10s, 99.1%] [18s, 100%]

Figure 5. 23 Phase contours in CFRTP composites with three inlets at 40 bar

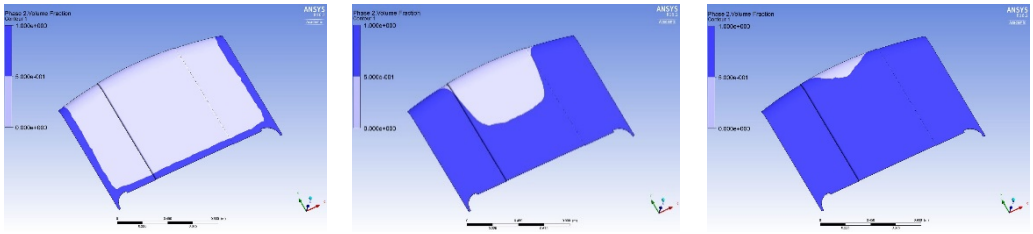

[1s, 13.4%] [2s, 76.1%] [5s, 96.7%]

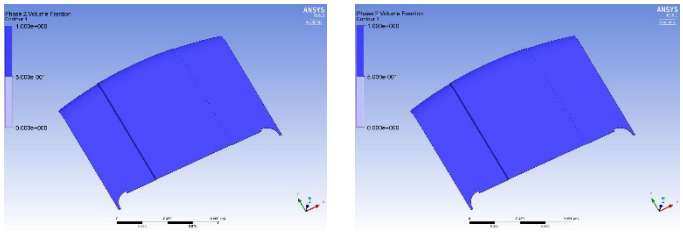

[10s, 99.9%] [13s, 100%]

Figure 5. 24 Phase contours in CFRTP composites with three inlets at 50 bar

Table 5. 2 Filling time and filling ratio at different pressures with three inlets

Molding temperature (℃)	Inlet pressure (bar)	Filling time (s)	Filling ratio (%)
140℃	10	20	72.7
	20	20	88.5
	30	20	96.0
	40	18	100
	50	13	100

Summary and Conclusions

In this study, carbon fabric reinforced PA6 composites were manufactured by vacuum assisted resin transfer molding (VaRTM) method. DSC analysis was conducted to evaluate polymerization kinetics of ε-caprolactam was for optimize molding process. Furthermore, the simulation results were compared with the experimental results, and the simulation of the automotive part was also performed to predict the molding conditions.

Carbon fiber reinforced thermoplastic (CFRTP) composites were prepared at five different temperatures and performed several mechanical tests. The content of unreacted monomer and water absorption of CFRTP composites are the least when the samples were molded at 140℃, and the samples which were molded at 140℃ shows best bending strength and modulus. However, the impact strength of 120℃ and 200℃ are higher than that of others, due to high content of unreacted monomer and poor impregnation. Moreover, crystallinity of VaRTM samples decreases as the molding temperature increases, and crystallinity of CFRTP is higher than that of PA6 due to carbon fiber which can act as nucleation agents.

DSC analysis was performed to evaluated polymerization and crystallization of polymerizing ε-caprolactam, polymerization and crystallization occurs simultaneously, and crystallinity during polymerization process decreases by increasing the heating rate due to deficient crystallization time. In order to investigate polymerization kinetics, polymerization peak can be separated from the exothermic peak using Gaussian distribution, and we use the first order autocatalytic reaction model for modeling the polymerization kinetics. It shows a very good fit which means that the model is suitable for describing the polymerization kinetics of ε-caprolactam.

Furthermore, we conducted isothermal scanning experimental. The results show that at lower temperature, crystallization and polymerization occurs at the same time, because at lower reaction temperature monomer could be trapped inside of the crystals before being able to polymerize. However, at high temperature, the growth of the chains is more significant than the formation of crystals.

Finally, numerical simulation was carried out for comparison with the results of experimental. The filling time obtained from the simulation results is similar to the experimental results. In the end, the simulation was also performed to evaluate the processing conditions of various shapes and sizes of automotive parts.

From the experimental and simulation results, it can be conclude that the optimum temperature for polymerization is 140~160℃, and the molding process

must be finished within 20 seconds regardless of the shapes and sizes of the samples.

Bibliography

[1] J. Takahashi and T. Ishikawa, "Current Japanese Activity in CFRTP for Industrial Application," *in International Conference on Textile Composites*, 2013: Leuven.

[2] J. Takahashi, K. Uzawa, and T. Matsuo, "Development of CFRTP for Mass Produced Automobile," 2010: Japan.

[3] Plastics Today, "New High-Pressure RTM Process for Carbon Fiber Composites Promises Economies of Scale," 2016 March 08 [cited 2016 November 1]; *Available from:* http://www.plasticstoday.com/.

[4] L. Khoun, D. Maillard, and M. N. Bureau, "Effect of Process Variables on the Performance of Glass Fibre Reinforced Composites Made by High Pressure Resin Transfer Moulding," *12th Annual Automotive Composites Conference and Exhibition (ACCE 2012)*, 2012.

[5] R. Chaudhari, P. Rosenberg, M. Karcher, S. Schmidhuber, P. Elsner, and F. Henning, "High Pressure RTM Process Variants for Manufacturing of Carbon Fiber Reinforces Composites," *19th International Conference on Composites Materials (ICCM 19)*, 2013: Canada.

[6] K. van Rijswijk and H. E. N. Bersee, "Reactive Processing of Textile Fiber-Reinforced Thermoplastic Composites - An Overview," *Composites Part a-Applied Science and Manufacturing*, vol. 38, pp. 666-681, 2007.

[7] K. R. Stewart, "Melt Polymerization Of BPA Cyclic Polycarbonate Oligomers - Rheokinetics Of Polymerization Relevant to Reactive Processing," *Abstracts of Papers of the American Chemical Society,* vol. 198, pp. 334-POLY, Sep 1989.

[8] R. Nagahata, J. J. Sugiyama, M. Goyal, M. Goto, K. Honda, M. Asai, *et al.*, "Thermal Polymerization of Uniform Macrocyclic Ethylene Terephthalate Dimer," *Polymer,* vol. 42, pp. 1275-1279, Feb 2001.

[9] S. Ahmadi, J. Morshedian, S. A. Hashemi, P. J. Carreau, and W. Leelapornpisit, "Novel Anionic Polymerization of epsilon-Caprolactam Towards Polyamide 6 Containing Nanofibrils," *Iranian Polymer Journal,* vol. 19, pp. 229-240, Mar 2010.

[10] M. R. Desai, M. V. Pandya, and C. S. Shah, "Effect of Initiator Structure on Physical and Thermal-Properties of Nylon-6," *Polymer International,* vol. 29, pp. 137-144, 1992.

[11] D. L. Wilfong, C. A. Pommerening, and Z. G. Gardlund, "Separation of Polymerization and Crystallization Processes for Nylon-6," *Polymer,* vol. 33, pp. 3884-3888, 1992.

[12] J. Kargerkocsis and L. Kiss, "Attemps of Separation of the Polymerization and Crystallization Process by Means of DSC Thermograms of Activated Anionic-Polymerization of epsilon-Caprolactam," *Makromolekulare Chemie-Macromolecular Chemistry and Physics,* vol. 180, pp. 1593-1597, 1979.

[13] J. Kargerkocsis and L. Kiss, "DSC Studies of the Activated Anionic-Polymerization of epsilon-Caprolactam in the Presence of Crown Compounds," *Journal of Polymer Science-Polymer Symposia,* pp. 67-71, 1981.

[14] K. J. Kim, D. S. Hong, and A. R. Tripathy, "Kinetics of Adiabatic Anionic Copolymerization of epsilon-Caprolactam in the Presence of Various Activators," *Journal of Applied Polymer Science,* vol. 66, pp. 1195-1207, Nov 1997.

[15] S. Pillay, U. K. Vaidya, and G. M. Janowski, "Liquid Molding of Carbon Fabric-reinforced Nylon Matrix Composite Laminates," *Journal of Thermoplastic Composite Materials,* vol. 18, pp. 509-527, Nov 2005.

[16] S. Mohammadian-Gezaz, I. Ghasemi, and A. Oromiehie, "Preparation of Anionic Polymerized Polyamide 6 using Internal Mixer: The Effect of Styrene Maleic Anhydride as a Macroactivator," *Polymer Testing,* vol. 28, pp. 534-542, Aug 2009.

[17] D. Zheng, G. S. Tang, H. B. Zhang, Z. Z. Yu, F. Yavari, N. Koratkar, *et al.*, "In Situ Thermal Reduction of Graphene Oxide for High Electrical Conductivity and Low Percolation Threshold in Polyamide 6 Nanocomposites," *Composites Science and Technology,* vol. 72, pp. 284-289, Jan 2012.

[18] Y. Gong, A. D. Liu, and G. S. Yang, "Polyamide Single Polymer Composites Prepared via in Situ Anionic Polymerization of epsilon-Caprolactam," *Composites Part a-Applied Science and Manufacturing,* vol. 41, pp. 1006-1011, Aug 2010.

[19] Y. Gong and G. S. Yang, "All-Polyamide Composites Prepared by Resin Transfer Molding," *Journal of Materials Science,* vol. 45, pp. 5237-5243, Oct 2010.

[20] G. Ben, A. Hirabayashi, K. Sakata, K. Nakamura, and N. Hirayama, "Evaluation of New GFRTP and CFRTP using epsilon Caprolactam as Matrix Fabricated with VaRTM," *Science and Engineering of Composite Materials,* vol. 22, pp.

633-641, Nov 2015.

[21] G. C. Ben and K. Sakata, "Fast Fabrication Method and Evaluation of Performance of Hybrid FRTPs for Applying Them to Automotive Structural Members," *Composite Structures*, vol. 133, pp. 1160-1167, Dec 2015.

[22] M. M. Davoodi, S. M. Sapuan, D. Ahmad, A. Ali, A. Khalina, and M. Jonoobi, "Mechanical Properties of Hybrid Kenaf/Glass Reinforced Epoxy Composite for Passenger Car Bumper Beam," *Materials & Design*, vol. 31, pp. 4927-4932, Dec 2010.

[23] J. Holbery and D. Houston, "Natural Fiber Reinforced Polymer Composites in Automotive Applications," *JOM*, vol. 58, pp. 80-86, 2006.

[24] N. Saba, M. T. Paridah, and M. Jawaid, "Mechanical Properties of Kenaf Fibre Reinforced Polymer Composite: A Review," *Construction and Building Materials*, vol. 76, pp. 87-96, Feb 2015.

[25] R. Alagirusamy and V. Ogale, "Development and Characterization of GF/PET, GF/Nylon, and GF/PP Commingled Yarns for Thermoplastic Composites," *Journal of Thermoplastic Composite Materials*, vol. 18, pp. 269-285, May 2005.

[26] W. Hufenbach, R. Bohm, M. Thieme, A. Winkler, E. Mader, J. Rausch, *et al.*, "Polypropylene/Glass Fibre 3D-Textile Reinforced Composites for Automotive Applications," *Materials & Design*, vol. 32, pp. 1468-1476, Mar 2011.

[27] U. K. Vaidya, F. Samalot, S. Pillay, G. M. Janowski, G. Husman, and K. Gleich, "Design and Manufacture of Woven Reinforced Glass/Polypropylene Composites for Mass Transit Floor Structure," *Journal of Composite Materials*, vol. 38, pp. 1949-1972, 2004.

[28] F. D. Ning, W. L. Cong, J. J. Qiu, J. H. Wei, and S. R. Wang, "Additive Manufacturing of Carbon Fiber Reinforced Thermoplastic Composites Using Fused Deposition Modeling," *Composites Part B-Engineering*, vol. 80, pp. 369-378, Oct 2015.

[29] H. Shaikh, S. K. H. Gulrez, A. Anis, A. M. Poulose, P. E. H. Qua, M. K. Yadav, *et al.*, "Progress in Carbon Fiber and Its Polypropylene- and Polyethylene-Based Composites," *Polymer-Plastics Technology and Engineering*, vol. 53, pp. 1845-1860, 2014.

[30] H. Adam, "Carbon Fibre in Automotive Applications," *Materials & Design*, vol. 18, pp. 349-355, Dec 1997.

[31] Wikipedia, t.f.e. "Monomer," 20 December 2016 [cited 2017 January 9]; *Available from:* https://en.wikipedia.org/wiki/Monomer.

[32] Wikipedia, t.f.e. "Caprolactam," 21 October 2016 [cited 2017 January 9]; *Available from:*https://en.wikipedia.org/wiki/Caprolactam.

[33] F. M. Al-Oqla, S. M. Sapuan, M. R. Ishak, and A. A. Nuraini, "A Decision-Making Model for Selecting the Most Appropriate Natural Fiber - Polypropylene-Based Composites for Automotive Applications," *Journal of Composite Materials*, vol. 50, pp. 543-556, Feb 2016.

[34] S. Jeyanthi and J. J. Rani, "Development of Natural Long Fiber Thermoplastic Composites for Automotive Frontal Beams," *Indian Journal of Engineering and Materials Sciences*, vol. 21, pp. 580-584, Oct 2014.

[35] M. Khalfallah, B. Abbes, F. Abbes, Y. Q. Guo, V. Marcel, A. Duval, *et al.*, "Innovative flax tapes reinforced Acrodur biocomposites: A new alternative for automotive applications," *Materials & Design*, vol. 64, pp. 116-126, Dec 2014.

[36] J. L. Thomason and G. Porteus, "An Investigation of Glass-Fiber Reinforced Polyamide 66 During Conditioning in Various Automotive Fluids," *Polymer Composites*, vol. 32, pp. 1369-1379, Sep 2011.

[37] J. Zhang, K. Chaisombat, S. He, and C. H. Wang, "Hybrid Composite Laminates Reinforced with Glass/Carbon Woven Fabrics for Lightweight Load Bearing Structures," *Materials & Design*, vol. 36, pp. 75-80, Apr 2012.

[38] H. L. Yin, X. Q. Peng, T. L. Du, and J. Chen, "Forming of Thermoplastic Plain Woven Carbon Composites: An Experimental Investigation," *Journal of Thermoplastic Composite Materials*, vol. 28, pp. 730-742, May 2015.

[39] S. S. Zhang, X. D. Wang, and D. Z. Wu, "Design and Fabrication of Long-Carbon-Fiber-Reinforced Polyamide-6/Nickel Powder Composites for Electromagnetic Interference Shielding and High Mechanical Performance," *Polymer Composites*, vol. 37, pp. 2705-2718, Sep 2016.

[40] M. X. Li, G. H. Lee, D. S. Lee, J. M. Jung, and W. I. Lee, "DSC Investigation and Modeling of the Polymerization for epsilon-caprolactam," 2016, Korea.

[41] S. Russo, S. Maniscalco, P. Moretti, and L. Ricco, "Fast-Activated Anionic Polymerization of epsilon-Caprolactam in the Bulk under Quasi-adiabatic Conditions: Comparison of Different Kinetic Models," *Journal of Polymer Science Part a-Polymer Chemistry*, vol. 51, pp. 4474-4480, Oct 2013.

[42] K. H. Lee and S. C. Kim, "Reaction-Induced Crystallization Kinetics during the Anionic-Polymerization of epsilon-Caprolactam," *Polymer Engineering and Science*, vol. 28, pp. 13-19, Jan 1988.

[43] J. Nagy, L. Reith, M. Fischlschweiger, and G. Steinbichler, "Influence of Fiber Orientation and Geometry Variation on Flow Phenomena and Reactive

Polymerization of Epsilon-Caprolactam," *Chemical Engineering Science,* vol. 128, pp. 1-10, May 2015.

[44] J. M. Kenny, "Determination of Autocatalytic Kinetic-Model Parameters Describing Thermoset Cure," *Journal of Applied Polymer Science,* vol. 51, pp. 761-764, Jan 1994.

[45] G. Liang and K. Chandrashekhara, "Cure Kinetics and Rheology Characterization of Soy-Based Epoxy Resin System," *Journal of Applied Polymer Science,* vol. 102, pp. 3168-3180, Nov 2006.

[46] J. J. E. Teuwen, A. A. van Geenen, and H. E. N. Bersee, "Novel Reaction Kinetic Model for Anionic Polyamide-6," *Macromolecular Materials and Engineering,* vol. 298, pp. 163-173, Feb 2013.

[47] C. W. Hirt and B. D. Nichols, "Volume of Fluid (VOF) Method for the Dynamics of Free Boundaries," *Journal of Computational Physics,* vol. 39, pp. 201-225, 1981.

[48] Wikipedia, t.f.e. "Darcy's law," 22 December 2016 [cited 2017 January 9]; *Available from:* https://en.wikipedia.org/wiki/Darcy's_law.

[49] N. Barhoumi, A. Maazouz, M. Jaziri, and R. Abdelhedi, "Polyamide from Lactams by Reactive Rotational Molding via Anionic Ring-Opening Polymerization: Optimization of Processing Parameters," *Express Polymer Letters,* vol. 7, pp. 76-87, Jan 2013.

[50] R. S. Dave, R. L. Kruse, K. Udipi, and D. E. Williams, "Polyamides from lactams via anionic ring-opening polymerization .3. Rheology," *Polymer,* vol. 38, pp. 949-954, Feb 1997.

[51] J. H. Byun, "Composites for future automotive," *KIMS-CRD Workshop on Composite Materials,* 2016.

현장중합을 이용한 CFRTP 복합재료 성형 공정의 모델링에 대한 연구

서울대학교 대학원
기계항공공학부
이 미 현

초 록

열가소성 수지 복합재료는 비강도가 높고, 내충격성이 좋을 뿐만 아니라, 재활용이 가능한 장점을 갖고 있기 때문에 이에 대한 많은 연구들이 이루어지고 있다. 그러나 열가소성 수지는 용융점 이상의 높은 온도에서도 점도가 높기 때문에 공정 방법에 있어 제한을 받는다. 자주 사용하는 열가소성 성형 방법에는 압출성형, 사출성형, 압축성형 등이 있는데 이러한 공정은 높은 온도 및 압력을 필요로 하는

단점이 있을 뿐만 아니라 단섬유 사용을 주로 하고 섬유 체적 함유율이 낮기 때문에 제품의 광범위한 응용에 있어서도 제한을 받는다. 열가소성 수지 기반 복합재료 수요가 증가하는 시점에서 섬유 함유율이 높고 저비용 공정 기술을 개발하는 것이 필요하다.

이 연구에서는 액체 성형 공정 중 하나인 진공 보조 수지 이송 성형 (VaRTM)을 이용하여 열가소성 수지 기반 복합재료를 제조하였다. VaRTM 공정은 주로 열경화성 수지의 성형에 사용되는 공정 기술로 점도가 높은 열가소성 수지 성형 공정으로는 적합하지 않다. 그러나 점도가 낮은 모노머를 이용하면 충분히 열가소성 수지 기반 복합재료를 제작 할 수 있다. 모노머는 일정한 촉매, 활성제, 온도 등 조건에서 분자량이 큰 폴리머로 중합 되기 때문에 이 원리를 이용하면 VaRTM 공정으로도 열가소성 수지 제품을 만들 수 있다.

폴리아미드6 (PA6)는 흔히 사용하는 공업용 폴리머 중 한 가지 폴리머로써 그 응용 범위가 광범위 하다. 카프로락탐은 PA6의 모노머로 낮은 온도에서도 점도가 낮기 때문에 액상 성형 공법으로 공정 할 수 있다. VaRTM 과정에서 카프로락탐은 촉매, 활성제 및 일정한 온도 조건에서 PA6 로 중합되는데 중합도는 보통 촉매 및 활성화제의 종류 및 사용 비율, 중합 온도 등의 영향을 받는다. 본 연구에서는 주로 중합 온도가 PA6 복합재료의 물성 및 중합 메커니즘에 주는 영향에 대하여 연구하였다. 실험 결과 중합 온도가 140℃ 일 때, 미반응

모노머가 가장 적고 함침 및 기계적 물성이 가장 좋은 것으로 나타났다.

본 연구의 또 다른 하나의 목적은 카프로락탐의 중합 메커니즘을 연구하는 것이다. 카프로락탐 중합 과정에서 결정화 과정이 동시에 일어나고 두 가지 과정 모두 발열 반응이기 때문에 단순히 중합 메커니즘을 연구함에 있어 어려움이 있다. 그러므로 중합 과정과 결정화 과정을 분리 해 놓은 후, 오로지 중합 과정에 대한 메커니즘을 연구하는 방법을 고안하였다. 모델링 결과 1차 자가촉매 반응 모델식으로 카프로락탐 중합 메커니즘을 정확히 모델링 할 수 있음을 확인하였고 시뮬레이션과 실험의 비교를 통하여 최적의 공정 변수를 제시하였다.

주 요 어 : 카프로락탐, 진공보조 수지이송성형, 시차주사열량계, 중합 메커니즘, 결정화도

학 번 : 2011-31286